Agricultural and Forest Meteorology 346 (2024) 109864

Contents lists available at ScienceDirect

Agricultural and Forest Meteorology

journal homepage: www.elsevier.com/locate/agrformet

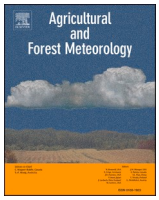

Dynamics of evapotranspiration from concurrent above- and below-canopy flux measurements in a montane Sierra Nevada forest

Sebastian Wolf [a,*], Eugénie Paul-Limoges [b,c], Dan Sayler [d], James W. Kirchner [a,c,e]

[a] Department of Environmental Systems Science, Physics of Environmental Systems, ETH Zurich, Zurich, Switzerland
[b] Department of Geography, University of Zurich, Zurich, Switzerland
[c] Swiss Federal Institute for Forest, Snow and Landscape Research (WSL), Birmensdorf, Switzerland
[d] Sagehen Creek Field Station, University of California – Berkeley, USA
[e] Department of Earth and Planetary Science, University of California – Berkeley, USA

ARTICLE INFO

Keywords:
Below-canopy ET
Subcanopy
Transpiration
Evaporation
Eddy covariance
AmeriFlux

ABSTRACT

Evapotranspiration (ET) from the land surface to the atmosphere is a major component of Earth's water cycle, and comprises both transpiration (T) of xylem water from plants and evaporation (E) of water from soils and vegetation surfaces. These two component fluxes respond differently to changes in temperature, water availability and atmospheric CO_2 concentrations. Concurrent eddy covariance (EC) measurements above and below forest canopies provide a promising approach to partition ET into E and T. However, below-canopy EC measurements are rare, and questions remain regarding their spatial variability, canopy coupling, and temporal dynamics. To address these challenges, we measured and partitioned ET over more than three years, using concurrent above- and below-canopy EC towers in a montane forest at Sagehen Creek in California's Sierra Nevada mountains. This is the establishing study for the AmeriFlux site US-SHC. The main environmental control for ET was available energy; other important controls were canopy & soil temperature, soil moisture, vapor pressure deficit, and wind speed. Below-canopy measurements at two locations within the above-canopy footprint were similar to one another, suggesting low spatial heterogeneity in understory ET near the creek at our Sagehen site. We observed a total forest ET of 606 ± 50 mm yr^{-1} with 275 ± 17 mm yr^{-1} measured in the understory (all mean ± SD) during the water years 2018–2020. Interannual variability in ET and T was small despite large variability in precipitation totals; thus the P–ET water balance was mainly driven by variations in water supply. Partitioning the components of total forest ET at Sagehen with concurrent EC measurements showed that on average, 67–74% of ET originated from T (47% from trees and 20–27% from understory vegetation), while 26–33% were from E (mostly from the understory). Our results demonstrate the potential of concurrent above- and below-canopy EC measurements for ET partitioning.

1. Introduction

Evapotranspiration (ET) from terrestrial ecosystems is a key component of Earth's water cycle, transporting approximately 60% of global precipitation (P) from the land surface to the atmosphere (Fisher et al., 2017; Oki and Kanae, 2006; Seneviratne and Stöckli, 2008). Evidence indicates that ET consists of, on average, about 61% (range 45–77%) transpiration (T) of xylem water from plants and about 39% (range 23–55%) evaporation (E) of water from wet soil and vegetation surfaces (Abbott et al., 2019; Nelson et al., 2020; Schlesinger and Jasechko, 2014). Although T and E are co-limited by atmospheric evaporative demand and soil moisture, they respond differently to changes in temperature, water availability, atmospheric CO_2 concentrations and land cover (Stoy et al., 2019). T is tightly coupled to gas exchange of plants, with stomata (leaf pores) regulating the rate of atmospheric carbon assimilation by photosynthesis and water loss by T (Anderegg et al., 2016). Plants may close their stomata, and thus reduce rates of T in response to increased atmospheric carbon dioxide (CO_2) concentrations (Betts et al., 2007; Cao et al., 2010; Keenan et al., 2013; Swann et al., 2016) or drought stress from water limitations in the soil and atmosphere (Carminati and Javaux, 2020; Choat et al., 2012; Kannenberg et al., 2022; Novick et al., 2019; Wolf and Paul-Limoges, 2023). E, by contrast, can increase with warmer temperatures as the vapor pressure deficit (VPD) in the atmosphere increases (Huntington, 2006),

* Corresponding author.
E-mail address: sewolf@ethz.ch (S. Wolf).

https://doi.org/10.1016/j.agrformet.2023.109864
Received 31 January 2023; Received in revised form 17 November 2023; Accepted 12 December 2023
Available online 23 December 2023

or can decrease at high VPD when it is constrained by limitations in soil water content (Or et al., 2013) and canopy-intercepted water. Thus, partitioning ecosystem ET into its components E and T is essential (Scott and Biederman, 2017) for separating stomatal responses from the confounding effects of non-stomatal contributions (Sulman et al., 2016), and for understanding the contrasting effects of a changing climate on surface temperature, regional cloud formation and local water availability (Roderick et al., 2015; Suni et al., 2015).

Among terrestrial ecosystems, forests contribute more than any other ecosystem type to global terrestrial ET, accounting for 44% of total ET and returning 26% of terrestrial P back to the atmosphere (Oki and Kanae, 2006). Forests also account for more than two-thirds of terrestrial gross primary production and store large quantities of carbon and water (Pan et al., 2013). Increasing atmospheric CO_2 concentrations and warmer climates may increase forest growth rates, with consequences for water availability, but the direction and magnitude of the effects remain highly uncertain (D'Orangeville et al., 2016; Way et al., 2021). Quantifying forest ET, its components, and their changes is thus pivotal for constraining uncertainties in water availability in a warming climate. This is of particular importance for montane forests as temperature increases in mountain regions are disproportionally larger than the global average (Pepin et al., 2015). Forest ET has been estimated to consist of roughly 55–70% T (temperate coniferous *vs.* deciduous forests) and 30–45% E (Schlesinger and Jasechko, 2014). Forest canopy interception losses have been estimated at about half of E, and tend to be higher in coniferous than in deciduous forests (Lian et al., 2022; Miralles et al., 2010; Zhong et al., 2022).

Forests are structurally complex ecosystems with distinct vertical layers and different functional properties in the understory and overstory (Misson et al., 2007). While total forest ET is regularly measured and modelled, the contributions from forest understories are highly uncertain (Thrippleton et al., 2018). Some evidence suggests that understory contributions (*i.e.* soil and vegetation) are on average one-third of total forest ET, yet the reported range (15–90%) is highly variable (Gobin et al., 2015). Understory ET contributions vary with forest density (*e.g.* based on leaf area index, LAI), with lower values in closed-canopy forests (Constantin et al., 1999) and higher values in more open-canopy stands (Baldocchi et al., 2004). The phenology of deciduous trees and understory vegetation can also affect the seasonally variable contributions of understory ET (Iida et al., 2009; Paul-Limoges et al., 2020). Understory contributions are also linked to forest composition (*e.g.* evergreen, deciduous, or mixed), climate (*e.g.* boreal, temperate, semi-arid, tropical), and soil properties (Misson et al., 2007). Ultimately, all these factors influence the available energy, light and water in the forest understory and hence affect understory contributions to total forest ET (Black and Kelliher, 1989; Jarosz et al., 2008; Thrippleton et al., 2018). Sometimes the water sources of understory and overstory vegetation are even decoupled (*i.e.,* trees may have access to groundwater that is inaccessible to grasses, and shrubs) thus reducing understory contributions to total ET during dry periods without P (Ma et al., 2020b; Scott et al., 2003).

Total forest ET at the ecosystem level, *i.e.* including soil, understory and overstory vegetation, can be directly measured above the canopy by the eddy covariance (EC) method, which quantifies turbulent biosphere-atmosphere exchange using high-frequency measurements of vertical wind velocity and water vapor concentrations (Baldocchi et al., 1988). However, EC measurements above the forest canopy cannot separate ET contributions from the understory (including the soil), nor can they partition the component fluxes of T and E. Both of these objectives typically require additional measurements by, *e.g.,* chambers (Kassuelke et al., 2022; Qubaja et al., 2020; Raz-Yaseef et al., 2012), weighing lysimeters (Hirschi et al., 2017; Liu et al., 2022; Perez-Priego et al., 2017; Sun et al., 2016), sap flow (Vandegehuchte and Steppe, 2013; Wilson et al., 2001), or alternatively require modelling approaches based on EC data and water use efficiency (Berkelhammer et al., 2016; Nelson et al., 2018; Perez-Priego et al., 2018; Scott and Biederman, 2017; Zhou et al., 2016), or high-frequency EC measurements for conditional sampling of turbulent eddies (Thomas et al., 2008) and for applying the flux-variance similarity approach (Scanlon and Kustas, 2012; Scanlon and Sahu, 2008; Skaggs et al., 2018; Stoy et al., 2019). These additional measurement methods, however, are typically limited to short campaigns, disturb plants and soil (*e.g.* chambers), are prone to potential sampling bias by only measuring selected plants and soil locations, or, in the case of sap flow measurements, are limited to woody plants and thus mostly overstory vegetation, with large uncertainties in converting sap flow densities to whole stand T fluxes (Čermák et al., 2004; Oishi et al., 2008; Peters et al., 2018; Poyatos et al., 2021).

A promising approach to overcome these limitations is concurrent above- and below-canopy EC measurements in forest and savanna ecosystems, which enable continuous direct measurements of both the forest floor and below-canopy contributions to ET (Misson et al., 2007). Such concurrent EC measurements can also be used for ET partitioning by subtracting below-canopy ET from above-canopy ET to estimate tree T, under the premise that ET in the canopy consists entirely of T during rain-free periods (Paul-Limoges et al., 2020). Previous studies quantifying understory contributions based on concurrent EC measurements (*i.e.* ET_{Below}/ET_{Above}) have reported widely varying estimates of understory ET as a fraction of total forest ET (ranging from 6 to 69%), with the smallest contributions found in temperate deciduous forests and the largest contributions in boreal larch forests or open oak-tree grass savannahs (Baldocchi et al., 2000, 1997; Black et al., 1996; Blanken et al., 2001; Constantin et al., 1999; Iida et al., 2009, 2020; Jarosz et al., 2008; Kelliher et al., 1997, 1998; Kilinc et al., 2013; Launiainen, 2010; Launiainen et al., 2005; Moore et al., 1996; Ohta et al., 2001; Perez-Priego et al., 2017; Scott et al., 2003; Sulman et al., 2016; Wilson et al., 2001). Overall, these contributions increase with the openness of the canopy (*i.e.* lower leaf area index, LAI) leading to higher amounts of available energy on the forest floor, and with higher VPD above the forest floor (Baldocchi and Ryu, 2011; Iida et al., 2009).

Only a few studies have so far used concurrent EC measurements to partition ET into its components by estimating tree T (*i.e.* $T \approx ET_{Above} - ET_{Below}$). According to these EC studies, the ratio of tree T to total forest ET (*i.e.* T/ET_{Above}) was reported to range from 67 to 95%, with the lowest values found in oak-grass savanna and the highest values in temperate or boreal deciduous forests (Black et al., 1996; Ma et al., 2020b; Paul-Limoges et al., 2020; Roupsard et al., 2006; Sulman et al., 2016; Wilson et al., 2001). In general, these T/ET ratios based on concurrent EC measurements are on the higher end of the typically reported range for forests based on various methods (55–70%; see *e.g.* Schlesinger and Jasechko, 2014), which could be linked to the underlying assumption that interception from trees (*i.e.* E from leaves and branches during and after P, and from dew) is minimal. Some studies account for that interception and short-term storage by excluding days of P and 1–5 days afterwards, assuming that E will become negligible and that T will dominate ET afterwards (Keenan et al., 2013; Knauer et al., 2018; Nelson et al., 2020; Sulman et al., 2016).

Overall, many questions remain regarding the wider applicability of concurrent above- and below-canopy EC measurements. Ongoing discussions in the literature include, *e.g.,* the effects of forest structure and density on advection and the decoupling of above- and below-canopy exchange (Jocher et al., 2018, 2017; Novick et al., 2014; Paul-Limoges et al., 2017; Thomas et al., 2013), the validity of existing cospectral models for below-canopy measurements (Chi et al., 2021), differences in source areas (footprints) between canopy layers (Baldocchi, 1997; Misson et al., 2007; Sulman et al., 2016), and the spatial variability of measurements below the canopy, linked to *e.g.* the heterogeneity of trees and forest gaps (Burns et al., 2014; Raupach and Shaw, 1982), or advective fluxes in complex topographies (Feigenwinter et al., 2008), which have been only rarely investigated so far, during singular seasons or short campaigns (Wilson and Meyers, 2001; Yang et al., 1999).

To address some of these questions and to quantify ET contributions

from the understory, this study uses more than three years of concurrent above- and below-canopy EC measurements from a montane forest at Sagehen Creek, California. More specifically, the objectives of this study are (i) to investigate the temporal dynamics of ET above and below the canopy, (ii) to quantify the below-canopy contributions to total ecosystem ET, (iii) to evaluate the multi-year spatial variability of below-canopy measurements, (iv) to quantify tree T from partitioned ET, and (v) to compare ET and the ecosystem water balance at Sagehen Creek, CA with other sites across the Sierra Nevada.

This is the establishing study for the AmeriFlux site US-SHC (Sagehen Creek Field Station), which has been initiated in summer 2017 as the first site measuring EC fluxes on the east side of the Sierra Nevada mountains. Sagehen is one of very few sites within AmeriFlux measuring concurrent below-canopy fluxes and to our knowledge, the only site reporting more than three years of ET using replicated below-canopy EC measurements.

2. Methods

2.1. Site characteristics

Sagehen Creek Field Station (39°25′55″ N, 120°14′28″ W, 1943 m a.s.l.) is located about 26 km north of Lake Tahoe and 12 km north of the town of Truckee on the east side of the Sierra Nevada Mountains in California. The station is within the Sagehen Experimental Forest and has been operated by the University of California, Berkeley since 1951 under a long-term special-use permit from the U.S. Forest Service. Sagehen Creek is a snowfall-dominated catchment of about 35 km^2 with an elevation range of 1877–2663 m from the lower culvert up to Carpenter Ridge (see *e.g.* Cooper et al., 2020; Kirchner et al., 2020). The field station is located in the lower catchment near Sagehen Creek in a broad U-shaped, west-east-oriented valley (slope of 1–3°) with gentle slopes (4–6°) towards the south and steeper slopes (10–20°) towards the north.

Sagehen has a continental Mediterranean climate with cold, wet winters and warm, dry summers (Fig. 1). Mean annual precipitation (MAP) is 827 mm yr^{-1} (1981–2010, NOAA-NCDC Climate Normals) with 88% falling during the wet season (>50 mm mo^{-1}) from October to April, largely as snow (about 500 mm yr^{-1} or 60% of MAP). Mean annual temperature (MAT) is 5.3° C and mean monthly temperatures range from –3.1° C in December to 14.7° C in July. The prevailing wind direction is along the valley towards the west-southwest (WSW) with secondary contributions from the east (based on our measurements and by DRI-WRCC, *see Section 2.3*).

Vegetation in the Sagehen basin is dominated by montane forests (about 90%), complemented by meadows and shrubs (Kirchner et al., 2020). The montane forest at lower elevations at Sagehen is characterized by coniferous trees with Sierra Lodgepole pine (*Pinus contorta* var. *murrayana*) dominating the wetter locations near the creek and Jeffrey pine (*Pinus jeffreyi*) at drier locations along the slopes. Around the Field Station and near the creek (see Figure S1), grasses, sedges and forbs grow in the forest understory. This patchy, locally dense forest is mixed with variably sized, irregular patches of open meadows. Due to the heterogeneous patterns in tree density and meadow patches, the overall vegetation distribution most closely resembles a woodland or an open forest. Accordingly, the MODIS Landcover IGBP Classification for the location of Sagehen Creek Field Station is for 'Woody Savanna', whereas most of the surroundings are classified as 'Evergreen Needleleaf Forest'. The age of trees near the station is about 50–140 years, with the oldest trees being Jeffrey pines along the slope north of the station. Tree height within the footprint of the above-canopy flux tower (see Section 2.2) is highly variable, with the mean height being estimated at about 15 m in

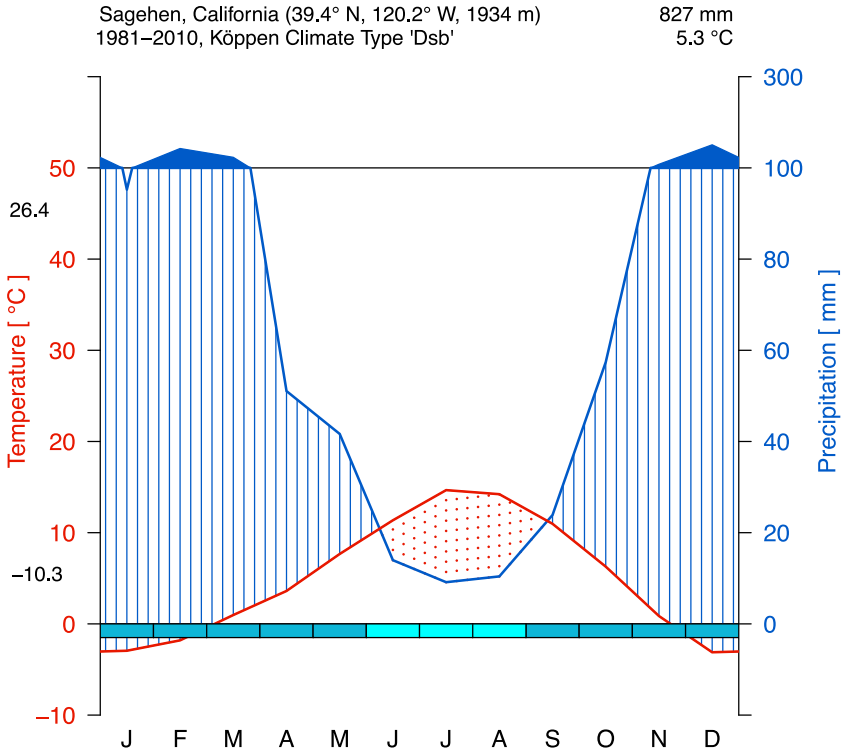

Fig. 1. Climate diagram after Walter and Lieth (1967) of Sagehen, California for the reference period 1981–2010 (Data source: NOAA-NCDC Climate Normals provided by the Western Regional Climate Center, https://wrcc.dri.edu/cgi-bin/cliMAIN.pl?ca7641). Shaded boxes on the x-axis denote months with certain frost (dark cyan) or probable frost (light cyan). The black numbers on the left y-axis refer to the daily minimum and maximum average temperature of the coldest and hottest month, respectively. According to the Köppen classification system, Sagehen belongs to the climate type 'Dsb', with a Mediterranean-influenced warm--summer continental climate, having cold and wet winters (see *e.g.* Kauffman, 2003). (For interpretation of the references to colour in this figure legend, the reader is referred to the web version of this article.)

2018. Grasses and sedges around the below-canopy (subcanopy) towers were about 0.40 m high during most of the growing season.

The soils in the Sagehen basin are classified as deep, well-drained acidic Alfisols in the Windy series, and have developed from weathered volcanic material. A typical soil profile in the basin consists of sandy loam that is dark greyish-brown and gravelly in the topsoil (0–60 cm), overlying a subsoil (60–115 cm) that is yellowish-brown and cobbly (Johnson and Needham, 1966; Mast and Clow, 2000). Surface geology in the basin is dominated by Quaternary alluvial, colluvial and glacial deposits that range from a few meters (or less) on most hillslopes up to >15 m at lower elevations near the creek. These deposits cover volcanic rocks (likely >400 m thick) from Tertiary Miocene–Pliocene andesitic and basaltic flows, with Cretaceous granodiorite below (Manning et al., 2012; Sylvester and Raines, 2017).

2.2. Experimental design, instrumentation and data acquisition

In June 2017, three triangular flux towers using the eddy covariance (EC) method were installed at Sagehen to measure the biosphere-atmosphere exchange of water vapor and energy. Our paired experimental design consisted of a 30 m high flux tower to measure the total ecosystem exchange above the forest canopy and two small flux towers within the forest understory measuring below-canopy (subcanopy) exchange (see Fig. 2). For simplicity, these three towers are referred to as 'AC' for the above-canopy measurements, and as 'BC1' and 'BC2' for the replicated below-canopy (subcanopy) measurements (see tower locations in Figure S1).

The micrometeorological measurement systems consisted of an open path infrared gas analyzer (EC150) combined with a three-dimensional sonic anemometer (CSAT3A) in a single instrument (IRGASON, Campbell Scientific, Logan, USA). Instruments were installed at a height of 30 m for the above-canopy measurements and 2 m for the below-canopy measurements. Data acquisition was conducted using a CR3000 datalogger combined with an AM16/32B multiplexer (Campbell Scientific, Logan, USA). Raw data were recorded at 10 Hz on 16 GB industrial CompactFlash cards (Swissbit C-320, Bronschhofen, Switzerland).

Ancillary meteorological measurements included air temperature and relative humidity (HMP155A, Vaisala, Vantaa, Finland), four-component net radiation (R_N; CNR4 with CNF4 ventilation unit, Kipp & Zonen, Delft, The Netherlands), photosynthetic photon flux density (*PPFD*; LI-190R, LI-COR, Lincoln, USA), and canopy temperature (SI-111 Infrared Radiometer, Apogee, Logan, USA). In the soil, we replicated three co-located measurements each at 5 cm depth for soil heat flux (*G*; HFP01, Hukseflux, Delft, The Netherlands) and soil temperature (TCAV Averaging Soil TC Probe, Campbell Scientific, Logan, USA). In addition, a soil profile with volumetric water content (*SWC*) and temperature was measured at 10 cm, 30 cm and 50 cm depth (CS650, Campbell Scientific, Logan, USA). At the above-canopy flux tower, a vertical profile of air temperature and relative humidity (HMP60, Vaisala, Vantaa, Finland) along with wind speed (03101 Wind Sentry, R. M. Young, Traverse City, USA) was measured at heights of 3.25 m, 13 m and 20 m since June 2018. This logarithmic profile complemented pre-existing long-term measurements of air temperature and relative humidity (HMP45AC, Vaisala, Vantaa, Finland), as well as wind direction and speed (05103 Wind Monitor, R. M. Young, Traverse City, USA) at a height of 6.5 m (since 2006) and 30 m (since 2009). These long-term measurements are

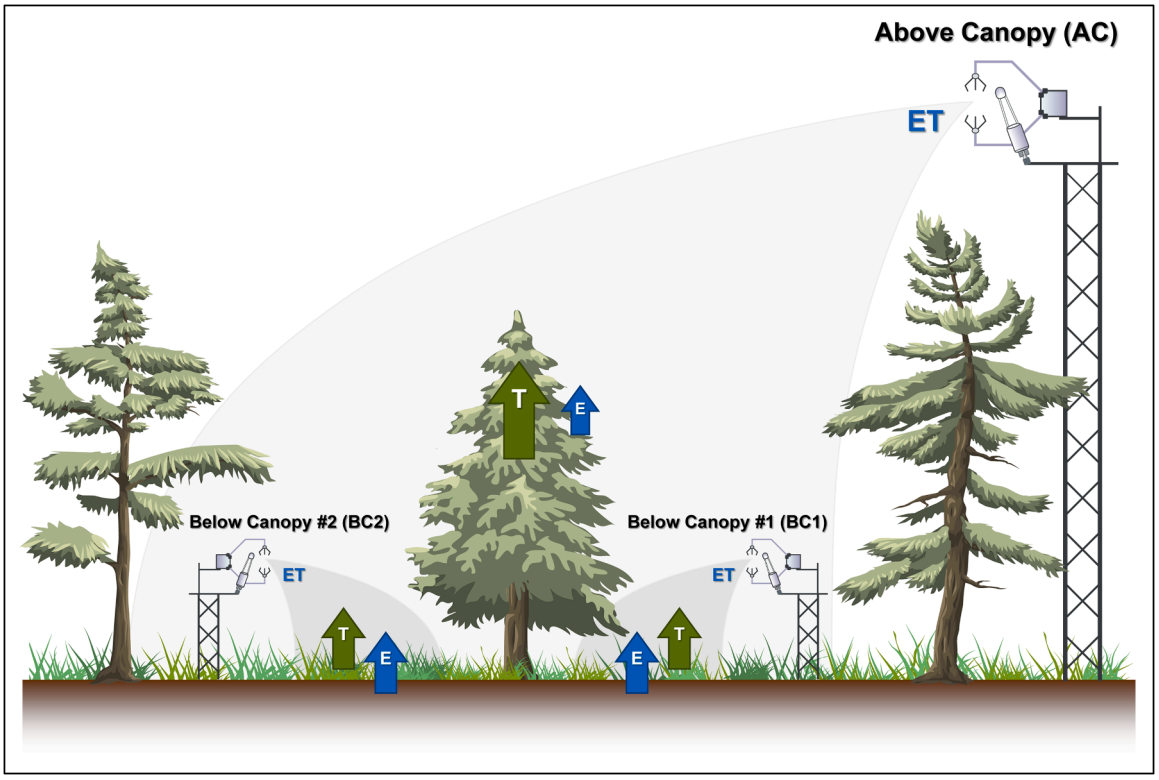

Fig. 2. Conceptual experimental design of concurrent above- and below-canopy measurements of evapotranspiration (ET) with the eddy covariance (EC) method at Sagehen Creek Field Station. Above-canopy (AC) measurements were conducted at 30 m height. Below-canopy (or subcanopy) measurements were conducted at the 'Below Canopy #1′ (BC1) and 'Below Canopy #2′ (BC2) towers at 2 m height. Only ET is directly measured by the EC method, not the component fluxes of transpiration (T) of plant xylem water and evaporation (E) of water on soil and vegetation surfaces. The contribution of trees to total ecosystem ET (measured above canopy) can be estimated as 'ET Trees ≈ ET Above Canopy – ET Below Canopy'. Assuming negligible E from the vegetation surface of coniferous trees (except following dew or rain), this estimate yields the partitioned T of trees. Grey shadings denote the footprint or source area measured by each tower. Please note that the sizes and distances are conceptual and not to scale, although the order of the towers in direction from the southwest (left) to the northeast (right) is according to the installation at Sagehen (see Figure S1). (For interpretation of the references to colour in this figure legend, the reader is referred to the web version of this article.)

maintained by the Field Station in collaboration with the Desert Research Institute (DRI), which processes and provides these data via the Western Regional Climate Center (WRCC, https://wrcc.dri.edu/cgi-bin/rawMAIN.pl?casagh). Similarly, P was measured near the above-canopy tower by DRI with a vibrating wire weight gauge (T-200B, GEONOR, Augusta, USA).

All of our meteorological measurements were made every 10 s and stored as half-hourly averages. Measurements by DRI-WRCC were stored as 10-min averages (or, for P, sums) using a CR1000 datalogger (Campbell Scientific, Logan, USA). The data acquisition started on June 20, 2017 and is currently still ongoing. The data presented in this study cover the period of June 21, 2017 to September 30, 2020, thus representing more than three water years (October to September).

All flux towers were powered by several 12 V batteries (GPL-31T, 105 Ah, Lifeline Batteries Inc., San Dimas, CA, USA), each connected to multi-bank automatic battery chargers (Guest Charge Pro 2731A and Marinco ChargePro 28,210, Marinco, Menomonee Falls, WI, USA). The flux tower measurements above the canopy at Sagehen have been part of the AmeriFlux network since 2017 (https://ameriflux.lbl.gov, Site-ID: US-SHC). Regular cleaning of the sensors was performed 1–2 times per week to ensure unbiased measurements. The IRGASONs were calibrated 1–2 times per year using nitrogen (99.998%, Linde Gas North America LLC, Bridgewater, USA), CO_2 reference standards provided by AmeriFlux, and a portable LI-610 Dew Point Generator (LI-COR, Lincoln, USA).

2.3. Flux data processing

2.3.1. EC processing and quality filtering

Raw high-frequency data were processed to half-hourly averages using the software EddyPro (v7.0.7, LI-COR, Lincoln, USA). Statistical tests for raw data screening of each half-hourly period were performed after Vickers and Mahrt (1997) and included spike detection and removal (max. 1% of time series), plausible range of measurements, and steady state criteria for horizontal wind. To correct for spectral attenuation, analytical transfer function approaches were applied to account for both high-pass (Moncrieff et al., 2004) and low-pass filtering effects (Massman, 2000, 2001) in the frequency response of raw fluxes (see *Section 2.4.1*). Block averaging was used to detrend the raw data. For tilt correction, we applied a planar-fit coordinate rotation (Wilczak et al., 2001) with four wind sectors for the above-canopy measurements to account for the complex terrain and tall, heterogeneous vegetation. A conventional double rotation (Kaimal and Finnigan, 1994) was used for the below-canopy measurements with lower wind speed conditions and more homogeneous terrain (see Rebmann et al., 2012). Turbulent half-hourly H_2O fluxes were calculated by Reynolds averaging from the covariance of vertical wind velocity with H_2O molar density, and were corrected for air density fluctuations (Webb et al., 1980). The storage flux from one-level tower measurements was added to obtain the net exchange of H_2O. Subsequently, half-hourly averaged fluxes were quality screened to exclude periods with: (1) optical sensor contamination, *e.g.* by snow or rain, frost, or dirt (based on IRGASON signal strength below 0.83–0.88, instrument-specific), (2) low data quality in stationarity and integral turbulence characteristic tests according to Foken and Wichura (1996) and Mauder et al. (2008), (3) fluxes outside a physically plausible range (*i.e.* <-200 and >800 W m^{-2} s^{-1}), (4) statistical outliers exceeding the $\pm$ 3 SD range of a 14-day running mean window, and (5) low turbulence conditions based on the standard deviation of vertical wind velocity (σ_w) as determined by Wutzler et al. (2018), with single-tower σ_w-thresholds of 0.150 m s^{-1} for the AC, 0.065 m s^{-1} for BC1, and 0.062 m s^{-1} for BC2. In addition to these general quality-filtering steps, we screened our data specifically for the analysis of below-canopy exchange (see Sections 2.3.2 & 2.3.3).

2.3.2. Decoupling assessment

Concurrent EC measurements above and below canopy are a powerful tool to quantify understory contributions to ecosystem fluxes, as well as decoupling related bias in the turbulent exchange between both canopy layers. Several studies have shown that the relationship between the standard deviation of vertical wind velocity (σ_w) measured above and below canopy can be used to determine decoupled periods (Chi et al., 2021; Jocher et al., 2018, 2017; Paul-Limoges et al., 2017; Thomas et al., 2013). This approach is considered a direct measure for turbulent exchange and has been suggested to be preferable over alternative measures such as friction velocity for subcanopy measurements in forests (Thomas et al., 2013). Both canopy layers are coupled as long as the relationship of above- and below-canopy σ_w is linear and decoupling occurs when this relationship breaks down. At Sagehen, we found a clear separation between the coupled and decoupled regimes for both below-canopy towers (see Figure S2). Although the decoupling thresholds below the canopy were relatively similar, the breakdown in linearity was more pronounced at BC1 (σ_w=0.056 m s^{-1}) compared to BC2 (σ_w=0.060 m s^{-1}). The latter also showed a lower decoupling threshold for the above-canopy measurements, with σ_w=0.240 m s^{-1} at BC2 *versus* σ_w=0.280 m s^{-1} at BC1. This indicated a stronger coupling of the BC2 below-canopy tower, which is located in a more open part of the forest understory and near the edge of a large meadow to the south (see Figure S1). Overall, these values observed at Sagehen were comparable to other recent studies (Jocher et al., 2018, 2017). We screened periods of decoupling by using the site-specific σ_w–thresholds for the below-canopy towers and the higher (*i.e.* more conservative) threshold linked to BC1 for the above-canopy measurements. Subsequent to the general quality screening including single-tower σ_w (see *Section 2.3.1*), these decoupled periods that were screened out accounted for 13.4%, 6.6% and 3.5% of measured data for AC, BC1 and BC2, respectively.

2.3.3. Counter-gradient transport

Measurements of turbulence below and within forest canopies are susceptible to counter-gradient transport through downward-moving eddies, when gradients indicate no (*i.e.* zero gradient) or upwards transport (Denmead and Bradley, 1985). For water vapor concentrations, such movements unrealistically indicate condensation below the canopy, when none should occur. To omit counter-gradient periods, we screened our below-canopy data for times of negative ET fluxes, when the measured air temperature exceeded the dew point temperature (see Paul-Limoges et al., 2020). These periods accounted for an additional 5.4% and 12.8% of measured below-canopy data that were screened out for BC1 and BC2, respectively.

2.3.4. Gap filling

The quantification of total ET requires the filling of gaps in the measured and quality-filtered data. After the full quality screening, 47% of good data remained for the above-canopy tower AC (80% and 15% of daytime and night-time data, respectively), 52% (70% daytime, 39% night-time) for the below canopy tower BC1, and 45% (67% daytime, 26% night-time) for BC2. These percentages of gaps are comparable to other flux tower sites using similar data quality screening criteria, see *e.g.* Wolf et al. (2011). Gaps in measured fluxes were filled by the marginal distribution sampling (MDS) approach of Reichstein et al. (2005) using the R package REddyProc (Wutzler et al., 2018). The same approach was used to also gap-fill meteorological variables (*e.g.* incoming shortwave radiation, air temperature) and other turbulent fluxes (*e.g.* sensible heat flux).

2.4. Evaluation of EC measurements

2.4.1. Spectral analysis

Analyzing ensemble cospectra for the frequency response of the open-path IRGASON sensors showed overall very limited signal attenuation in the measured fluxes at Sagehen (see Figure S3). The cospectra of the above-canopy measurements were relatively close to the Kaimal ideal for flat terrain (Kaimal et al., 1972) with only minor deviations of

the gas fluxes (*i.e.* H_2O and CO_2) compared to the temperature cospectra. Cospectra for both below-canopy sites showed distinct amplification in the high-frequency range (stronger at BC1 than BC2) compared to the ideal cospectra from Kaimal, *i.e.* larger than usual contribution of small, fast moving eddies. This applied to all fluxes and was not limited to the gas fluxes (*i.e.* also for sensible heat), which indicated that these deviations originated from the location of the measurements below the canopy rather than signal attenuation from the measurement setup itself. Interactions of the wind field with tree elements (*e.g.* trunks, branches, leaves) dissipate energy from large, slow moving eddies and increase fine-scale (*i.e.* high-frequency) turbulence within and below forest canopies, resulting in higher contributions of small, fast moving eddies in the wake of these elements – a 'spectral short cut' mechanism (Finnigan, 2000). Accordingly, the turbulent exchange within plant canopies may be attenuated in the low-frequency part of the cospectra (Brunet, 2020) rather than exhibiting instrumentation-related attenuation in the high-frequency range (see *e.g.* Foken et al., 2012). At Sagehen (see Figure S3), the cospectra showed such an attenuation in the low-frequency range at BC1, yet to a minor extent only. At BC2, by contrast, the cospectra showed a slight amplification in the low-frequency range and some attenuation in the mid-frequency range. The differing cospectra at BC2 might be related to the lower density of adjacent trees and potentially greater contributions from the open meadow towards the South (see Figure S1).

Measuring with open-path instruments at Sagehen, we used the analytical Massman approach (Massman, 2000, 2001) to correct for spectral attenuation in the high-frequency range. An evaluation of various instrument setups and spectral corrections showed that this approach performs well for IRGASON instruments, which typically require only minimal spectral corrections (Polonik et al., 2019). By contrast, it was recently suggested that below-canopy measurements with enclosed-path sensors require distinct, site-specific cospectral models to avoid the underestimation of annual CO_2 fluxes (Chi et al., 2021). This emphasizes a need for systematically investigating spectral signal attenuation with various instrumental setups for potentially developing alternative cospectral models for below-canopy EC measurements in forests.

2.4.2. Advection

To ensure sufficient turbulent mixing and to account for advection, we screened our measurements for low-turbulence conditions based on friction velocity (*see Section 2.3.1*) and the standard deviation of vertical wind velocity, specifically during periods of decoupled exchange between above- and below-canopy fluxes (*see Section 2.3.2*). Based on this screening, periods with insufficient turbulent mixing were excluded. In addition, we analyzed profiles of wind speed and direction (see Figure S4), wind shear between above and below the canopy (see Figure S5), and distributions of wind fields (see Figures S6 & S7) for evidence of advection and katabatic flows at Sagehen. We observed much lower mean wind speeds at both below-canopy towers, with 0.27 $\pm$ 0.01 m s^{-1} at BC1 and 0.41 $\pm$ 0.01 m s^{-1} at BC2, compared to 1.89 $\pm$ 0.05 m s^{-1} measured above the canopy (AC). Profile measurements of wind speed showed limited evidence for katabatic flow during nighttime (see Figure S5). No directional wind shear (*i.e.* direction difference) was observed between above-canopy (215 $\pm$ 3°) and below-canopy winds at BC1 (216 $\pm$ 3°, see Figure S5), which are both located near the creek (distance of ~20 m) and thus along the bottom of the west-east oriented valley. However, a pronounced mean wind shear of about 35° towards the south was measured between above-canopy and below-canopy winds at BC2 (181 $\pm$ 7°). This is likely related to (i) the larger distance of BC2 from the creek (~60 m towards the south), to (ii) topography-related differences in wind fields within the Sagehen valley, and to (iii) the more open vegetation cover near BC2, with a large open meadow just south of the BC2 tower (see Figure S1), resulting in lower surface roughness. Additional evidence for (i) and (ii) is higher nighttime frequencies in wind direction along the creek (BC1) or towards the creek (BC2), indicating katabatic flow along the orographic slope, and additional evidence for (iii) is the higher wind speed observed at BC2 compared to BC1 (see Figures S6 & S7).

2.4.3. Energy balance closure

The energy balance closure of half-hourly data comparing radiative ($R_N - G$) and turbulent measurements (sensible heat flux plus latent heat flux) of available energy (*AE*) above the canopy at Sagehen was 65% (R^2=0.82). We found a slightly higher closure of 67% (R^2=0.79) during the dry season and a lower closure of 55% (R^2=0.79) during the wet winter season (see Figure S8). Based on the heterogeneity of vegetation patterns at our site, specifically the variability in tree density and meadow patches (see *Section 2.1*), we think that this low energy balance closure is largely related to differences in source areas for the radiative and turbulent measurements at the above-canopy tower . While radiative measurements (*i.e.* R_N and G) were dominated by the signal of open meadow near the above-canopy tower (see Figure S1), the signal of the turbulent flux measurements represents the full vegetation distribution of trees and meadow patches within the footprint of this patchy woodland ecosystem (*see Section 3.2* & Fig. 4). Such differences in measured source areas related to landscape heterogeneity are considered an important cause for the lack of energy balance closure across the global flux tower network (Foken, 2008; Leuning et al., 2012; Stoy et al., 2013). We also evaluated the averaging of above- and below-canopy radiative measurements (*i.e.* R_N and G) for better representing the source areas of the turbulent fluxes. This averaging yielded a slightly better closure of 68% (R^2=0.76) and particularly increased closure during the wet season (74%, R^2=0.67), yet less so for the dry season (64%, R^2=0.74). However, the coefficients of determination (R^2) were consistently lower using the averaged radiative measurements, likely linked to the large magnitude and variability of combined above- and below-canopy measurements. Assessing energy balance closure for below-canopy measurements is generally challenging due to the patchiness in the forest understory (see Figure S1) and thus large spatiotemporal variability of trees' shading effects on the single-point radiative measurements, which are non-representative for the measured turbulent fluxes (Launiainen et al., 2005). These differences in radiative and turbulent measurements of *AE* are particularly pronounced during times with low sun angles, such as in the morning/afternoon or during non-summer seasons. For both our below-canopy locations, energy balance closure was about 27% (R^2=0.71, not displayed) and was particularly low (only 8–10%, R^2=0.24–0.31) during the wet season (*i.e.* shoulder and winter seasons), when shading effects resulted in larger variability in radiative measurements ($R_N - G$) compared to turbulent measurements ($LE + H$) of *AE*.

2.5. Footprint analysis

To estimate the spatial extent and location of surface source areas (*i.e.* footprint or fetch) for the measured turbulent exchange, we performed footprint analysis using the model by Kljun et al. (2015). This footprint model applies a two-dimensional parametrization based on a scaling approach for the crosswind distribution of the flux footprint, with the explicit consideration of surface roughness length. The Flux Footprint Prediction (FFP) by Kljun et al. (2015) provides the extent, width and shape of footprint estimates (as contour lines) as well as densities of source contributions (*i.e.* '*heat map*'). The model and code for FFP is available at http://footprint.kljun.net and we used the R version of the code for our analysis. Please see Kljun et al. (2015) for a discussion of the limitations and uncertainties of this footprint model, including a comparison with other footprint models. We limited our footprint analysis to daytime data as nighttime ET only played a minor role for total ET at Sagehen (*i.e.* less than 15% above and 12% below canopy).

2.6. Contributions of below-canopy and partitioning of ET

We used concurrent above- and below-canopy EC measurements to

quantify the contributions from below the canopy to total ecosystem ET. The below-canopy measurements integrate $E_{Understory}$ from the soil and understory vegetation surfaces (*i.e.* 'physical' components of ET) as well as $T_{Understory}$ from the understory vegetation (*i.e.* 'biological' components from plants). In addition to those understory components, the above-canopy EC measurements also integrate the contribution from the trees, more specifically T_{Tree} and E_{Tree} from tree surfaces (see Fig. 2). All below-canopy contributions are directly measured as ET_{Below} by the small (below-canopy) flux towers, while total ecosystem ET (including the below-canopy flux) is measured above the canopy by the tall tower. This concept to quantify the contributions has two main requirements: (i) the turbulent exchange of the above- and below-canopy layer is coupled and measured accordingly as total ecosystem exchange by the above-canopy EC system. (ii) The sampling areas are overlapping, *i.e.* the below-canopy towers are within the 'footprint' or source area of the above-canopy measurements. To ensure the two requirements for quantifying the contribution of the below-canopy fluxes and the trees to total ecosystem ET (see above), we screened our data for periods of decoupling (see *Section 2.3.1*) and analyzed the footprints of all flux towers (see *Sections 2.5 & 3.2*).

Furthermore, concurrent measurements above and below the canopy can be used to estimate the contribution of trees to total ecosystem ET (ET_{Above}, measured above canopy) as 'ET Trees ≈ ET Above Canopy – ET Below Canopy'. Assuming negligible E_{Tree} of intercepted water from the vegetation surface of trees following dew and precipitation, this estimate yields the partitioned T_{Tree}. We also quantified the influence of canopy interception and E_{Tree} from wet tree surfaces (*i.e.* leaves, branches and trunk) at Sagehen by excluding days of P and up to five days afterwards (see Table S1) based on the assumption that E_{Tree} will become negligible thereafter (Keenan et al., 2013; Knauer et al., 2018; Nelson et al., 2020; Sulman et al., 2016). These estimates for canopy interception were then used for obtaining corrected ratios of T/ET at the seasonal to annual scale.

Based on our experimental setup with concurrent EC measurements and site-specific seasonal characteristics, we also estimated other partitioning components of total forest ET at Sagehen. While ET_{Below} cannot be directly partitioned into $E_{Understory}$ and $T_{Understory}$ from our measurements, some estimates can be made from seasonal considerations. During winter, the understory vegetation at Sagehen becomes senescent and it can be assumed that there is no $T_{Understory}$ when the ground is snow-covered (see Fig. 5). Consequently, measured ET_{Below} over the snow surface during winter is only $E_{Understory}$, *i.e.* sublimation. Based on this observation-informed estimate of sublimation, we can derive the remaining annual ET_{Below} relative to total forest ET. During the rest of the year (May to October), understory vegetation (mainly grass) is covering most of the ground (as can be determined from PhenoCam imagery, see *Section 2.8* and Fig. 8) at these particular locations. Based on these observations, which follow recurring seasonal patterns at Sagehen every year (see Figs. 8 and S11), we conservatively assumed that half to two-thirds of measured ET_{Below} during the dry season at Sagehen is from $T_{Understory}$, and the rest $E_{Understory}$ from soil and vegetation-intercepted water. Nonetheless, this is an estimate based on our season-specific observations at Sagehen and we thus propagate the effects of this range (*i.e.* $T_{Understory}$ is 50–67% of dry season ET_{Below}) into the derived T/ET ratios for the total ecosystem partitioning estimates (see Table S2). Combining these below-canopy estimates of $T_{Understory}$ and $E_{Understory}$ with the estimates of E_{Tree} from interception (see above and Table S1), enables observation-constrained estimates of all partitioning components for this specific site. Because most of the other components are well constrained from our experimental setup (*i.e.* concurrent above- and below-canopy measurements, continuous phenological observations) and seasonal patterns (*i.e.* snow cowered ground), we can report such a well-constrained observation-based estimate for $T_{Understory}$, which could otherwise not be determined at all.

We measured ET_{Below} with two flux towers below the canopy at Sagehen to also represent and quantify the spatial variability within the below-canopy (subcanopy) layer. Unless noted otherwise, we averaged the measurements of both below-canopy flux towers to quantify mean values for this understory layer.

2.7. Auxiliary measurements and data

Leaf area index (LAI) at Sagehen was measured with an LAI-2000 (LI-COR, Lincoln, USA) in mid-June 2018. To represent the variability within the forest, LAI was assessed from 30 measurements (24 times signal and 6 times reference) throughout the forest understory near the below-canopy flux towers. Two levels of LAI were measured in the understory, (a) just the tree canopy without ground vegetation and (b) total LAI including the ground vegetation (mostly grasses). LAI for the tree canopy was 1.58 ± 0.09 and total forest LAI including the grasses was 3.63 ± 0.11 (mean of both: 2.61 ± 0.10).

Vegetation phenology was tracked using networked digital cameras (PhenoCams). These measurements are part of the PhenoCam network (https://phenocam.nau.edu) and were installed at Sagehen at the tower above the canopy (*i.e.* AC, PhenoCam site 'sagehen') and the tower #2 below the canopy (*i.e.* BC2, PhenoCam site 'sagehen2') in October 2017, and at the tower #1 below the canopy (*i.e.* BC1, PhenoCam site 'sagehen3') in May 2019. The digital camera images were recorded half-hourly and stored on the PhenoCam network as well as on an ETH Zurich server. The separate color information in the images (*i.e.* RGB) is used to derive the green chromatic coordinate (GCC) for characterizing the activity of vegetation (Richardson et al., 2018). These processed data are available from the PhenoCam network (Seyednasrollah et al., 2019) and we use the 1-day summary product of all valid images for our analysis in this study, if not noted otherwise, at the 90th percentile of the distribution across all pixel). Estimates for phenophase transition dates indicate the median start of greenness rising and falling based on GCC (see Richardson et al. 2018).

2.8. Statistical analyses and general conventions

All statistical analyses (linear regression analysis, correlation analysis) were performed using the base package of the statistics software R, version 4.0.5 (R Foundation, www.r-project.org). Daytime data were defined as incoming shortwave (solar) radiation >10 W m^{-2} s^{-1}. Unless noted otherwise, we averaged the aggregated (*i.e.* daily, monthly, annual) measurements of both below-canopy flux towers to quantify mean values for this canopy layer.

For the analyses of the environmental controls we used linear regression analysis, reporting the explained variances in percent or as adjusted R^2 values. The multivariate analyses in these regressions were done including interactions among all considered variables. We also evaluated the averaging of environmental controls from above and below the canopy (*i.e.* calculating the mean of control variables such as AE) to improve the quantification of explained variance in ET_{Above} by better representing the source areas of the turbulent fluxes. This additional analysis was motivated by the heterogeneity of vegetation in the footprint/source area measured above the canopy (see Figs. 4 and S1), and because of related discrepancies between radiative and turbulent measurements (see *Section 2.4.3*).

3. Results

3.1. Environmental conditions

The water year 2017 (Oct. 2016 to Sep. 2017) was among the wettest on record with a total annual P of 1678 mm yr^{-1}, about double the 1981–2010 climatological mean for Sagehen (827 mm yr^{-1}, see Table 1). While P in 2018 was close to normal (+11%), the water year 2019 was wetter than average (1186 mm yr^{-1} or +43%). In comparison, 2020 was exceptionally dry at Sagehen (579 mm yr^{-1} or −30%) and should be considered a drought year, which was similar to the

Table 1
Annual and seasonal total precipitation (P), mean air temperature (Tair), evapotranspiration (ET) measured above and below the canopy, and transpiration (T) derived as T_{Tree}=ET_{Above}–ET_{Below} at Sagehen Creek Field Station during the water years (Oct.–Sep.) 2018–2020. Meteorological data for the reference period 1981–2010 are based on NOAA-NCDC Climate Normals provided by the Western Regional Climate Center (WRCC). Wet Season was defined as months with >50 mm of P during the reference period. ET_{Below} denotes the mean of both below-canopy towers and T_{Tree} denotes the estimate from ET_{Above} – ET_{Below}, with the ratio T/ET calculated relative to ET_{Above}. PET was calculated after Penman–Monteith by fixing surface resistance to zero, assuming no or only a negligible stomatal component (Fisher et al., 2011).

Year	Season	Period	Σ P [mm]	P [%]	Tair [° C]	ET_{Above} [mm]	ET_{Below} [mm]	T_{Tree} [mm]	T/ET [%]	PET_A [mm]	PET_B [mm]	P−ET [mm]
1981–2010*	Water Year	Oct. – Sep.	827	100	5.3	–	–	–	–	–	–	–
	Wet season	Oct. – Apr.	728	88	0.5	–	–	–	–	–	–	–
	Dry season	May – Sep.	99	12	11.8	–	–	–	–	–	–	–
2018	Water Year	Oct. – Sep.	919	100	5.5	648	291	357	55	1321	591	271
	Wet season	Oct. – Apr.	844	92	0.3	233	64	169	73	420	74	611
	Dry season	May – Sep.	75	8	12.8	415	228	187	45	901	517	−340
2019	Water Year	Oct. – Sep.	1186	100	4.5	619	277	342	55	1244	547	567
	Wet season	Oct. – Apr.	1032	87	−0.2	195	49	146	75	390	69	837
	Dry season	May – Sep.	154	13	11.1	424	228	196	46	855	478	−270
2020	Water Year	Oct. – Sep.	579	100	5.5	551	258	293	53	1332	563	28
	Wet season	Oct. – Apr.	511	88	0.4	169	51	116	69	435	68	342
	Dry season	May – Sep.	68	12	12.8	382	205	177	46	897	495	−314
2018–2020#	Water Year	Oct. – Sep.	895 ± 304	100	5.2 ± 0.6	606 ± 50	275 ± 17	331 ± 33	54 ± 1	1299 ± 48	567 ± 23	289 ± 270
	Wet season	Oct. – Apr.	796 ± 264	89 ± 3	0.2 ± 0.3	199 ± 32	55 ± 7	144 ± 27	72 ± 3	415 ± 23	70 ± 3	597 ± 248
	Dry season	May – Sep.	99 ± 48	11 ± 3	12.2 ± 1.0	407 ± 22	220 ± 13	187 ± 10	46 ± 1	884 ± 26	497 ± 20	−308 ± 35

* NOAA-NCDC Monthly Normals (Source: WRCC).
\# values indicate the mean ± standard deviation.

2012–2015 California drought (616 ± 64 mm yr^{-1}). Snow cover typically lasted from late November until late April, with the exception of 2019, when it persisted well into May (see Fig. 3c). The timing of the melt-out of snow during spring varied by up to four weeks between years and determined the decline of soil moisture during the dry season. After this decline, near-surface soil moisture (10 cm depth) stayed relatively constant and only started to increase with the first isolated storms in late summer (see Fig. 3c). Low soil moisture persisted longer at 30 cm depth

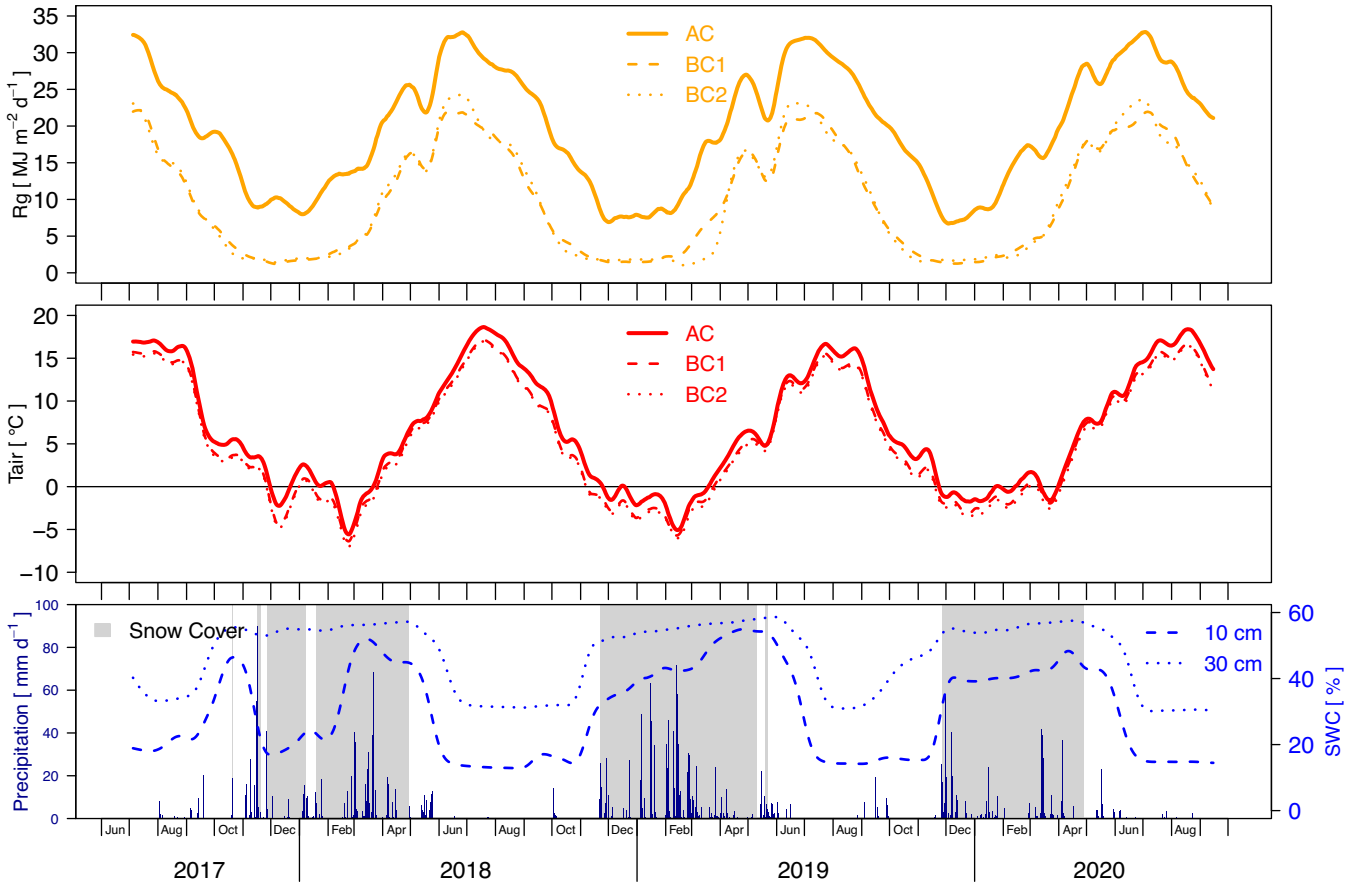

Fig. 3. Daily total incoming solar radiation (R_G), mean air temperature (Tair), total precipitation, and mean volumetric soil water content (SWC) measured above the canopy (AC) and at the two below-canopy towers (BC1 and BC2) during 2017–2020. All lines show 30-day running means. Grey shaded areas denote periods of snow cover on the ground as derived from PhenoCam imagery at BC2. (For interpretation of the references to colour in this figure legend, the reader is referred to the web version of this article.)

and in general during the dry seasons in 2018 and 2020.

Air temperatures during the water years 2017, 2018 and 2020 were close to average with 5.4–5.5° C, whereas the wet year 2019 was much colder (4.5° C, see Table 1). Annual total incoming solar radiation (R_G) varied by less than 5% (or max. 360 MJ m^2 yr^{-1}) between the years 2018–2020 measured above the canopy, and less than 3% (or max. 197 MJ m^2 yr^{-1}) measured below the canopy (see Fig. 3a). Total available energy ($AE = R_N – G$) above and below the canopy varied by only 1–2% (76–98 MJ m^2 yr^{-1}) across these years.

Albedo at Sagehen was predominantly determined by the periods of snow cover (see Figure S9). During the periods with snow cover from 2017 to 2020, the mean albedo was 0.26 ± 0.10 at the above-canopy tower (*i.e.* AC), while an albedo of 0.47 ± 0.15 and 0.52 ± 0.14 was measured for the below canopy towers BC1 and BC2, respectively (Note: averages based on December 1st to April 15th to remove bias from transition periods). During the period without snow cover, albedo was 0.13 ± 0.03 at the AC tower, 0.24 ± 0.05 at BC1 and 0.23 ± 0.05 at BC2. Overall mean albedo from 2017 to 2020 at Sagehen was 0.18 ± 0.10 measured above the canopy and 0.33 ± 0.17 measured below the canopy (mean of BC1 and BC2 with values of 0.31 ± 0.16 and 0.34 ± 0.17, respectively).

3.2. Footprint assessment

The surface source areas contributing to above-canopy (AC) measured turbulent fluxes during daytime showed a bimodal distribution along the valley, with the main contributions from WSW and secondary contributions from ENE (Fig. 4). Cumulative spatial contributions (80% contour) extended about 350 m to the WSW and 300 m to the ENE, with a smaller extent to the slopes on the south (~200 m) and north (~120 m). However, the highest densities of contributed fluxes (see '*heat map*' in right panel of Fig. 4) originated from within a distance of only 50 m around the tower. Overall, half of the flux contributions measured at Sagehen above the canopy were within 100 m from the tower. The below-canopy measurements at BC1 and BC2 had smaller and more evenly distributed source areas of about 20–30 m surrounding the towers. The highest densities of contributions measured below the canopy (see '*heat map*' Figure S10) were within only 5–10 m. Measurements from the below-canopy towers were within about the 60% contour of the above-canopy measurement footprint (distance of about 130 m from AC to BC2). Tower BC1 is located closer to the AC and thus more often within the higher density contributions measured above canopy. The two below-canopy towers had non-overlapping source areas during the majority (*i.e.* up to 80%) of our measurements.

3.3. Seasonal dynamics of ET

ET at Sagehen showed strong seasonality, with daily totals of 0.8 ± 0.7 mm d^{-1} (mean ± SD) measured below the canopy and 1.8 ± 1.1 mm d^{-1} above the canopy (Fig. 5). ET rapidly increased during spring, particularly after the melt-out of snow in May. Maximum daily ET of 2.7 mm d^{-1} and 5.0 mm d^{-1} was reached in July, with mean dry season (May to Sep) ET of 1.5 ± 0.6 mm d^{-1} and 2.7 ± 0.9 mm d^{-1} for below- and above-canopy measurements, respectively. ET substantially decreased in September and October, with December and January being typically the months with the lowest ET (close to zero), depending on the timing of synoptic weather patterns. Mean wet-season (Oct to Apr) daily ET was 0.3 ± 0.1 mm d^{-1} below and 0.9 ± 0.5 mm d^{-1} above the canopy. During the wet season, daily ET never exceeded 1.0 mm d^{-1} below the canopy, while this was rather common above the canopy. Considering just the periods with snow cover during winter (see Fig. 3), we still measured notable daily ET_{Below} of 0.2 ± 0.1 mm d^{-1}. As the understory vegetation was senescent and the soil was covered by snow, this ET_{Below} can be considered an estimate of sublimation. Compared to the annual total ET measured at Sagehen (see Table 1), sublimation from the snow surface within the forest understory accounted for about 10% of annual ET_{Below}, or 5% of total annual ET_{Above}.

Despite the large interannual variability in P during 2018–2020 at Sagehen (895 ± 304 mm yr^{-1}), annual ET was relatively stable at 606 ± 50 mm yr^{-1} above the canopy and 275 ± 17 mm yr^{-1} below the canopy (see Table 1). During the dry-season months of May to September, about 80% of annual ET_{Below} and 67% of annual ET_{Above} occurred. Only the dry year 2020 showed a notable reduction in daily ET to 2.88 mm d^{-1} (–11%) above and 1.63 mm d^{-1} (–9%) below the canopy during the

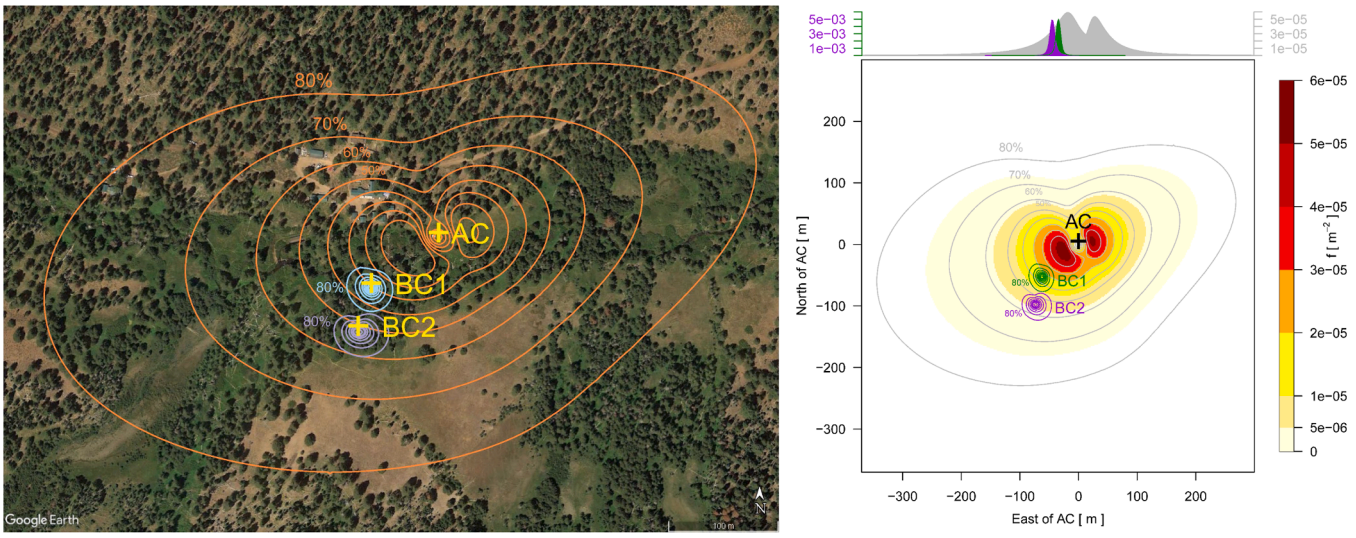

Fig. 4. Footprint climatology of daytime turbulent exchange after Kljun et al. (2015) for above-canopy (AC) and below-canopy (BC1 & BC2) measurements at Sagehen Creek Field Station from 21 June 2017 to 30 September 2020. Contour lines denote cumulative source area contributions (in steps of 10%) and crosses mark the locations of the towers. The background imagery in the left panel was recorded on 13 July 2016 (Google Earth). The right panel shows densities of source contributions (*i.e.* '*heat map*' of footprint function values) normalized per square meter (m^{-2}), with histograms of the maximum West-East densities displayed at the top. The colors of the histograms correspond to the colors of the contour lines, with gray referring to the above-canopy tower. Please note the different scaling of both panels as well as the differing orders of magnitudes in the histograms of the right panel (*i.e.* smaller source areas result in higher densities per unit area). A similar '*heat map*' for the below-canopy towers BC1 and BC2 can be found in the Supplement (Figure S10). (For interpretation of the references to colour in this figure legend, the reader is referred to the web version of this article.)

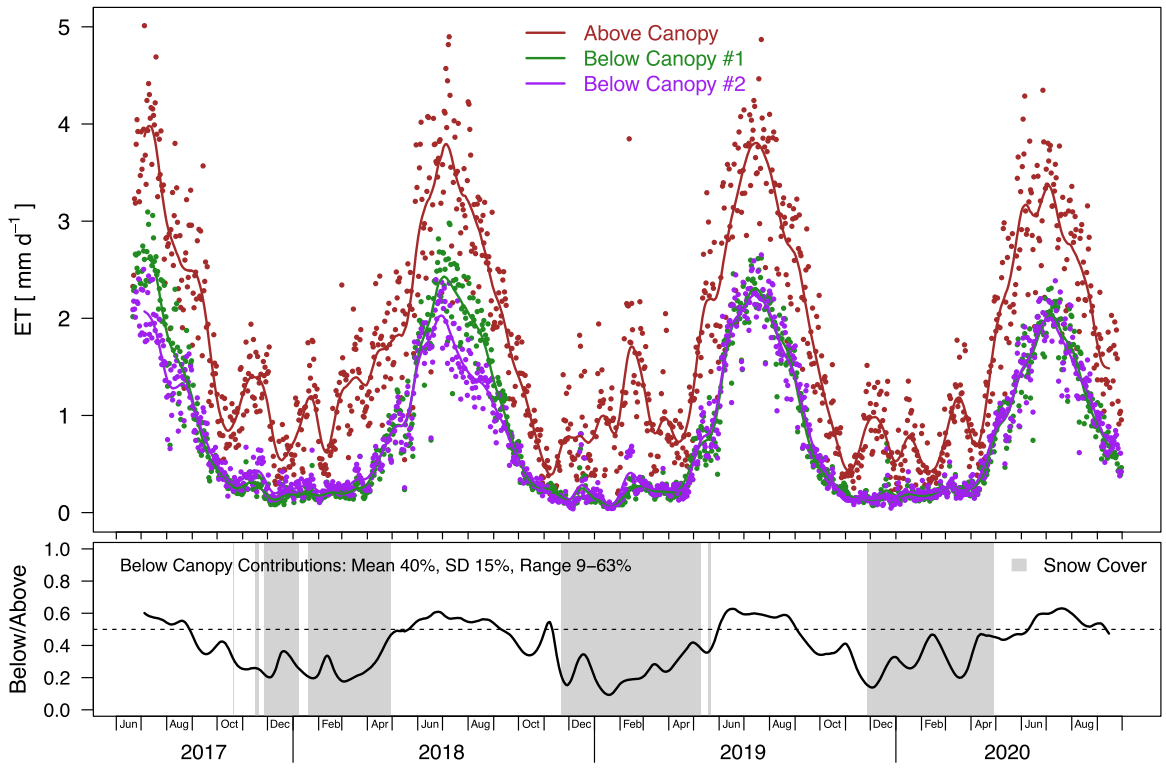

Fig. 5. Daily total evapotranspiration (ET) measured above the canopy (AC) and at the two below-canopy flux towers (BC1 & BC2) for 2017–2020. Points denote daily totals and lines denote 30-day running means. The lower panel shows the daily contributions of below-canopy to above-canopy ET as 30-day running means. Numbers denote the overall statistics of the contributions. Grey shaded areas denote periods of snow cover on the ground as derived from PhenoCam imagery at BC2. (For interpretation of the references to colour in this figure legend, the reader is referred to the web version of this article.)

summer months of June to August (see Fig. 5), compared to the nearly normal summer of 2018 (see *Section 3.1*).

Daily contributions from below the canopy to total ecosystem ET (see Fig. 5b) were on average 40 ± 15% and ranged from 9% in winter to 63% in summer. Below-canopy contributions were typically highest during June, except during the dry year 2020 when they peaked in mid-July. After their peak, below-canopy contributions declined along with the vegetation activity in the forest understory (see Fig. 8). Only during the summer months of June to August did ET_{Below} contribute more than half (57 ± 3%) of ET_{Above}. During the remainder of the year, ET_{Above} was dominated by contributions from the forest canopy, in particular during the snow-covered period in winter.

3.4. Environmental controls of ET

The main environmental control of half-hourly ET_{Above} was available energy (AE=R_N–G), which explained 51.6% of the variance (linear regression analysis, incoming solar radiation 'R_G' explained 50%). Soil temperature at 5 cm depth was the strongest residual predictor with 26.6%, followed by *VPD* with 15.9%, wind speed with 4.9%, and soil moisture (*SWC*) at 50 cm depth with 4.2%. Considering interactions, these five environmental controls together explained 77.0% of the variance in half-hourly ET_{Above}. During the dry summer months of June to August, ET_{Above} increased linearly with AE (R^2=0.62, single predictor), canopy temperature (R^2=0.42), VPD (R^2=0.34) and wind speed (R^2=0.14) but showed no apparent relationship with soil moisture. Below the canopy, *AE* was also the main control of half-hourly measured ET_{Below} (explaining 74.7% of the variance), closely followed by R_G (73.8%). Besides *AE*, the strongest residual predictors were soil moisture at 10 cm depth with 8.8%, soil temperature at 5 cm depth with 8.3%, VPD with 5.5%, and wind speed with 1.6%. Together these five factors explained 86.0% of the variance in half-hourly ET_{Below}. During the dry summer months, ET_{Below} increased linearly with AE (R^2=0.78), canopy temperature (R^2=0.54), VPD (R^2=0.38) and wind speed (R^2=0.09), but like ET_{Above}, showed no apparent relationship with soil moisture. Overall, this suggests similar limitations and water use strategies of understory vegetation and trees for this wet location near the creek.

Canopy temperature was also an important singular control on ET and explained more variance in ET (46.7% and 56.9% for above- and below-canopy measurements, respectively) than soil temperature did (34.3% and 27.0%, respectively). However, as a residual predictor of AE, canopy temperature explained less variance with 10.2% and 4.1% for above- and below-canopy measured ET, respectively, likely related to the fact that AE integrates canopy temperature already. Replacing soil temperature with canopy temperature in the multivariate analyses of the five most important environmental controls resulted in marginally lower (above canopy, 73.3%) or higher (below canopy, 88.1%) explained variance for half-hourly measured ET. Unlike *AE* and R_G, it is important to note that the causality of temperature variables and ET is multidirectional because the canopy and soil temperature are also influenced by evaporative cooling (*i.e.* ET).

The averaging of above- and below-canopy measurements for the environmental controls (see *Section 2.8*) of *e.g. AE, VPD* and *SWC* increased the variance of half-hourly ET_{Above} explained by *AE* to 60.0%. The same applied to VPD and SWC, each of which explained by itself (*i.e.* as a single factor) a substantially larger fraction of the variance in ET_{Above} when averaged across sensors of above- and below-canopy measurements. In comparison, averaging near-surface soil temperature and wind speed yielded negligible improvements in the explained variance of half-hourly ET_{Above}. No improvement was found using across-tower averages of environmental controls in a multivariate linear regression model for ET_{Above} at Sagehen.

3.5. Spatial dynamics of below-canopy measured ET

Half-hourly ET_{Below} measurements (*i.e.* at BC1 and BC2) were

strongly correlated (Spearman's ρ=0.86, R^2=0.75 with linear regression analysis), despite the two different locations in the heterogeneous forest understory (see Figure S1) and non-overlapping source areas (see Section 3.2 & Fig. 4). Comparing the daily totals of ET_{Below} at the two locations indicated only minor differences (Fig. 6). Although ET_{Below} was slightly higher at BC1 (0.84 ± 0.78 mm d^{-1}) than at BC2 (0.80 ± 0.68 mm d^{-1}; linear regression, BC2 slope of 1.11, R^2=0.94, Spearman's ρ=0.97), these differences were statistically insignificant and were limited to periods in mid-summer (July and August) of 2017 and 2018 (see Fig. 5). Mean water-year ET_{Below} from 2018 to 2020 was nearly the same at BC1 (278 ± 25 mm yr^{-1}) and BC2 (272 ± 11 mm yr^{-1}). Accordingly, the measurements at these two separate locations in the forest understory suggested limited spatial variability of ET_{Below} at Sagehen, at least for these relatively wet locations near the creek. The differences in ET_{Below} during summer 2017 and 2018 might be linked to soil and vegetation disturbances during and following the installation of instrumentation, as these differences were not observed in subsequent years (see Fig. 5). Comparative phenological observations (see *Section 3.7*) were only available since May 2019 at BC1 and thus did not provide insights into the vegetation disturbance hypothesis.

3.6. Tree T and ET partitioning

Using the concurrent above- and below-canopy measurements of ET, we estimated the T_{Tree} at Sagehen (see *Section 2.6*). The environmental controls of half-hourly T_{Tree} were similar to those observed for above- and below-canopy ET (see *Section 3.4*), although weaker. During the dry summer months, T_{Tree} increased linearly with AE (R^2=0.23, single predictor), canopy temperature (R^2=0.28), VPD (R^2=0.25) and wind speed (R^2=0.15), but also showed no apparent relationship with soil moisture. In other words, atmospheric evaporative demand (*i.e.* VPD) is more relevant than soil moisture for T_{Tree} at this wet location.

Daily totals of T_{Tree} were on average 0.9 ± 0.5 mm d^{-1}, with lower rates of 0.7 ± 0.4 mm d^{-1} during the wet season and higher rates of 1.2 ± 0.5 mm d^{-1} during the dry season (Fig. 7). T_{Tree} was lowest during the winter months and highest (up to 2.8 mm d^{-1}) in July. After the peak, T_{Tree} typically remained high until late August, except during the dry year 2020, when the highest rates of T were reached in early June and declined afterwards.

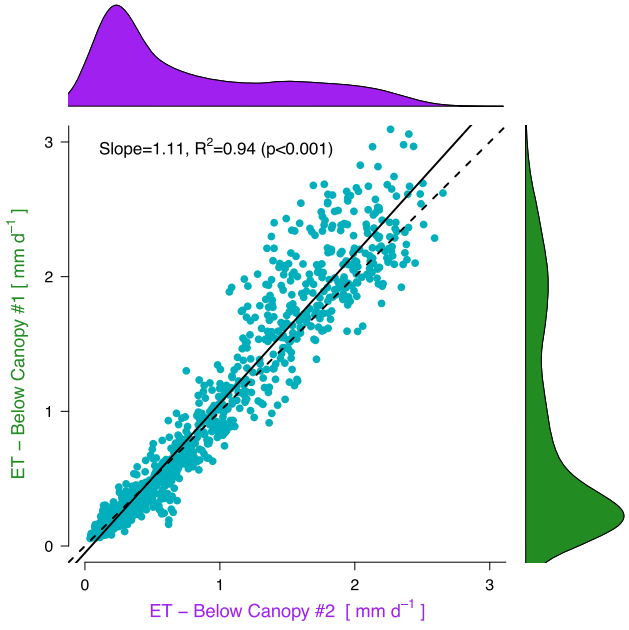

Fig. 6. Daily total evapotranspiration (ET) measured at the two below-canopy flux towers (BC1 & BC2) for 2017–2020. The solid line denotes the linear regression fit and the dashed line shows the 1:1 relationship between measurements at both towers. Marginal histograms show kernel density plots of daily ET for each tower.

Annual totals of T_{Tree} were relatively stable, averaging 331 ± 33 mm yr^{-1}, and were lowest during the dry year 2020 (293 mm yr^{-1}). During the dry season, total T_{Tree} was on average 187 ± 10 mm yr^{-1}, about 30% higher than during the wet season (144 ± 27 mm yr^{-1}). Overall, seasonal variations in T_{Tree} were substantially smaller than those in ET_{Above} as the coniferous trees remained photosynthetically active throughout the winter (see Fig. 8).

The daily contributions of T_{Tree} to total ecosystem ET_{Above} (T/ET) ranged from 37% to 91% and averaged 60 ± 15% (Fig. 7). T_{Tree} dominated daily ET_{Above} during the wet winter season from October to April (71 ± 10%), particularly when the ground was covered by snow, although seasonal analyses excluding interception effects indicated that about 11% of this value is due to sublimation of canopy-captured snow (see *Section 2.6* and Table S1). During the dry summer months of June to August, contributions of daily T_{Tree} were less than half of ET_{Above} (43 ± 3%). Based on seasonal and annual totals (see Table 1), the average (uncorrected) T/ET ratio was 46 ± 1% during the dry season, 72 ± 3% during the wet season, and overall 54 ± 1% during the water years 2018–2020. Correcting the T/ET ratios for canopy interception and E_{Tree} from wet tree surfaces (see *Section 2.6* and Table S1) showed that these effects became negligible three days after P events and yielded T/ET ratios of 44 ± 2% during the dry season, 63 ± 3% during the wet season, and 47 ± 2% overall for water years 2018–2020 (see Table S1). Accordingly, canopy interception played only a minor role of ~2% of total ET_{Above} during the dry summer season at Sagehen, when 80% of ET_{Below} and 67% ET_{Above} occurred. During the wet season, the effect of E_{Tree} was 9–11% and persisted beyond three days because P was dominated by snow.

Partitioning the components of total forest ET at Sagehen yielded averages of 47% for tree T_{Tree}, 7% for E_{Tree} from interception in the tree canopy, and 46% for ET_{Below}. While ET_{Below} cannot be directly partitioned into $E_{Understory}$ and $T_{Understory}$ from our measurements, some estimates can be made from seasonal considerations (see *Section 2.6* and Table S1). ET_{Below} during winter was dominated by $E_{Understory}$ from the snow surface (*i.e.* sublimation) and accounted for about 10% of total ET_{Below}, or 5% of total ET_{Above} (see Section 3.3). During the rest of the year, the remaining ET_{Below} (41% of total ET_{Above}) was likely dominated by $T_{Understory}$ from the dense grasses in the understory (see Section 2.7), but this could not be exactly quantified without additional measurements. However, based on observation-informed assumptions at Sagehen, we estimated $T_{Understory}$ as 50–67% of understory ET during the time without snow-cover (see *Section 2.6*) and thus $T_{Understory}$ was ≈ 20–27% of total ET_{Above}. Consequently, total forest T (from trees and understory grasses) was about 67–74% and total forest E was 26–33% of forest ET during the water years 2018–2020 (see Table S2). While the coniferous trees at Sagehen accounted for about two thirds (64–70%) of total T, only 22–28% of total E originated from the tree canopy.

It is important to note that the actual numbers of our assumption for $T_{Understory}$ (see above and *Section 2.6*) only play a minor role for the total forest T/ET ratio as $T_{Understory}$ is overall a small component of total forest ET at Sagehen. Even stretching this assumption to the possible maximum (*i.e.* $T_{Understory}$ is 50–100% of ET_{Below}) would only increase the total $T_{Understory}$ up to 20–41%. Or in other words, no more than 41% of total forest ET can theoretically originate from $T_{Understory}$ at this site.

Relative to total annual P, our measurements indicated a total T of 46–50% during the water years 2018–2020, with transpiration from coniferous trees accounting for 32% of total P, and total E accounting for 17–22% of total P (with 5% of total P being intercepted by, and subsequently evaporated from, the tree canopy; see Table S2).

3.7. Vegetation activity from phenological observations

Phenological vegetation activity (GCC, 90th percentile) was more

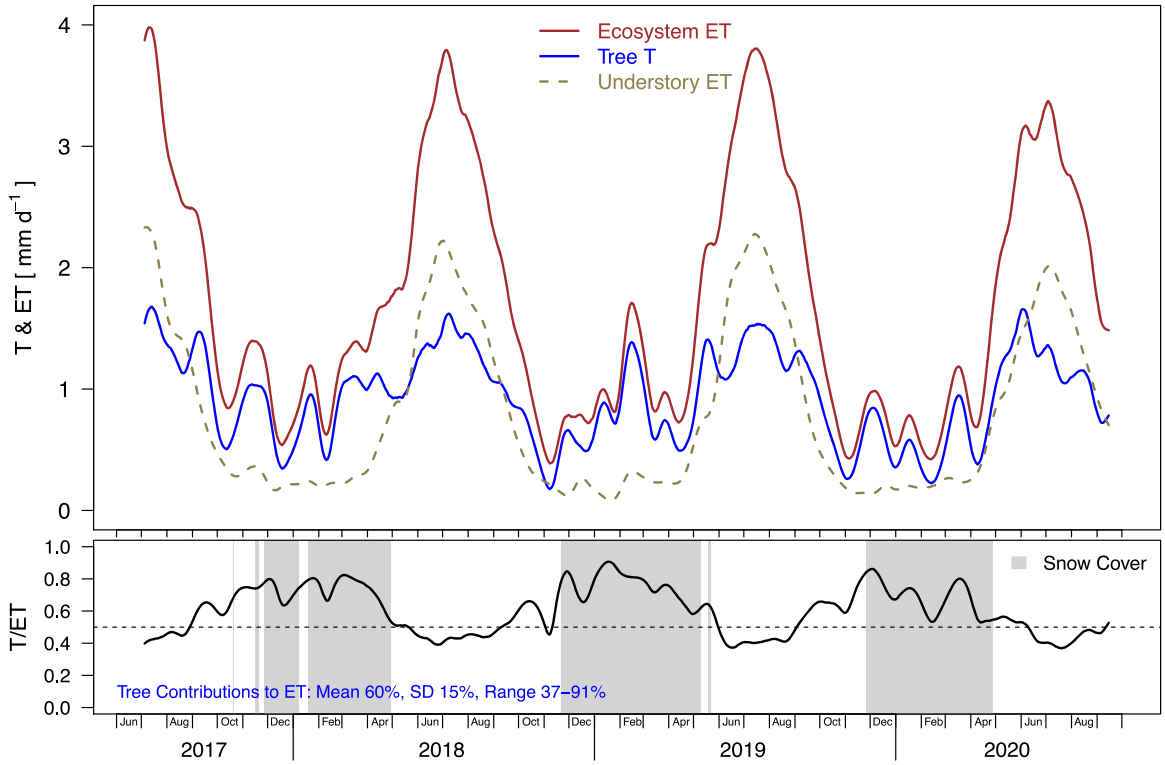

Fig. 7. Daily total ecosystem evapotranspiration (ET) measured above the canopy (ET_{Above}), understory ET measured below the canopy (ET_{Below}), and partitioned tree transpiration (T) from above- and below-canopy eddy covariance measurements ($T = ET_{Above} - ET_{Below}$) for June 2017 through September 2020. Lines denote 30-day running means. The lower panel shows tree contributions to total ecosystem ET (T/ET) and numbers denote the overall statistics of these contributions. Grey shaded areas denote periods of snow cover on the ground. A similar figure with the mean seasonal cycle across years can be found in the Supplement (Figure S11). (For interpretation of the references to colour in this figure legend, the reader is referred to the web version of this article.)

variable in the grasses at the below-canopy sites than in the evergreen trees measured from above the canopy (Fig. 8). The peak in phenological vegetation activity for the forest canopy occurred in May and the peak for the forest understory grasses occurred in June each year. Compared to summer, lower (but persistent) vegetation activity was observed for the forest canopy during the winter months. No vegetation activity was found for the understory vegetation from November to April each year, when the grasses were senescent or the ground was covered by snow.

Despite large differences in environmental conditions between years (see *Section 3.1*), the magnitude and extent of phenological vegetation activity was similar across years, both for the grasses in the understory and for the forest canopy. The only exception was the forest understory during the wet year 2019, when vegetation activity in spring started about 10–14 days later but also lasted an equivalent time longer in fall.

Relating daily vegetation activity from phenological observations (GCC) with daily ET totals (via linear regression analysis) showed that ET generally increased with GCC, but large differences were found between above- and below-canopy measurements. While above-canopy GCC (GCC_{Above}) explained only 29% of the variance in daily ET_{Above}, below-canopy GCC (GCC_{Below}) explained 80% and 82% of the variance in ET_{Below} at BC1 and BC2, respectively. Thus, we combined the strong relationship of GCC_{Below} with the environmental controls of *AE* and VPD (see *Section 3.4*) in a simple linear, multivariate regression model, which explained 95% and 90% of daily ET_{Below} for BC1 and BC2, respectively. Partitioned T_{Tree} also linearly increased with GCC_{Above}, but the relationship was only weak (R^2=0.11). The weak relationship above canopy (for both ET_{Above} and T_{Tree}) is likely related to the overall small seasonal variability in phenology of the evergreen coniferous trees (compared to the grasses in the understory) and confounding effects from *e.g.* understory vegetation seen by the PhenoCam.

Comparing the mean seasonal cycle of vegetation activity with T_{Tree} from the forest canopy and ET measured above and below the canopy showed a recurring pattern in the timing of ET and T_{Tree} at Sagehen (see Figure S11). Vegetation activity typically peaked early during the growing season, with new growth of needles in the forest canopy in May and the regrowth of grasses in the understory during June. In comparison, peak T_{Tree} and ET were only reached later, subsequent to peak insolation and with increasing VPD during July.

3.8. Water balance (P-ET)

The difference between water supply by P and water loss by ecosystem ET to the atmosphere (P–ET water balance) showed a surplus of 271 mm yr^{-1} during the close-to-average water year 2018 and 567 mm yr^{-1} during the wet year 2019, while it was close to zero (28 mm yr^{-1}) during the dry year 2020 (Table 1 & Fig. 9). Despite these large differences in total annual P–ET, time-series analysis (Fig. 9) showed a similar slope of decline in cumulative P–ET across years during the dry season starting by about mid to late May (15.05.2018, 03.06.2019, 18.05.2020), indicating similar rates of ET from vegetation water use across years at Sagehen. The onset of this persistent decline concurred with the pronounced increase of total ecosystem ET (see Fig. 7) and the peak period of vegetation activity (see Fig. 8). In addition, the onset of this decline was related to the disappearance of snow cover (see Fig. 3), which occurred on average 23 ± 4 days before during the years 2018–2020. Besides the timing of melt-out, the relatively stable total annual ET at Sagehen across years (see *Section 3.3*) indicates that the P–ET water balance at this wet location in the lower catchment is mainly determined by water supply from P and scarcely by vegetation water use. Accordingly, the P–ET water deficit during the dry year 2020 (*vs.* relatively normal year 2018) is almost equivalent to the precipitation deficit.

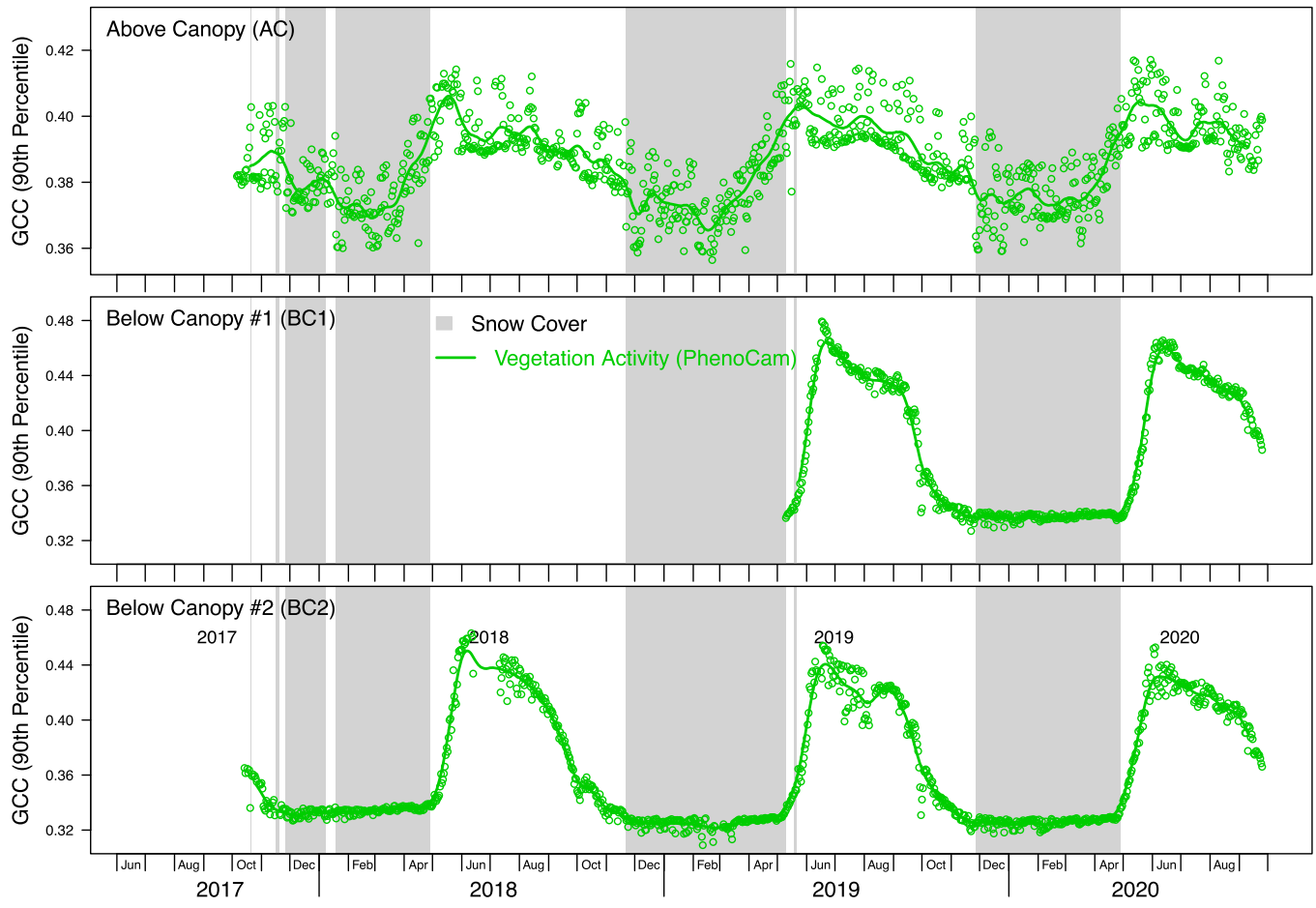

Fig. 8. Daily vegetation activity from phenological observations of green chromatic coordinate (GCC) at the 90th percentile of the distribution across all pixels. Points denote daily means and lines denote 30-day running means. Grey shaded areas denote periods of snow cover on the ground as derived from PhenoCam imagery at BC2. Please note the different scaling of the y-axis for the above- and below-canopy measurements. Measurements at BC1 only started in May 2019. A similar figure with the mean seasonal cycles measured above and below the canopy across years can be found in the Supplement (Figure S11). (For interpretation of the references to colour in this figure legend, the reader is referred to the web version of this article.)

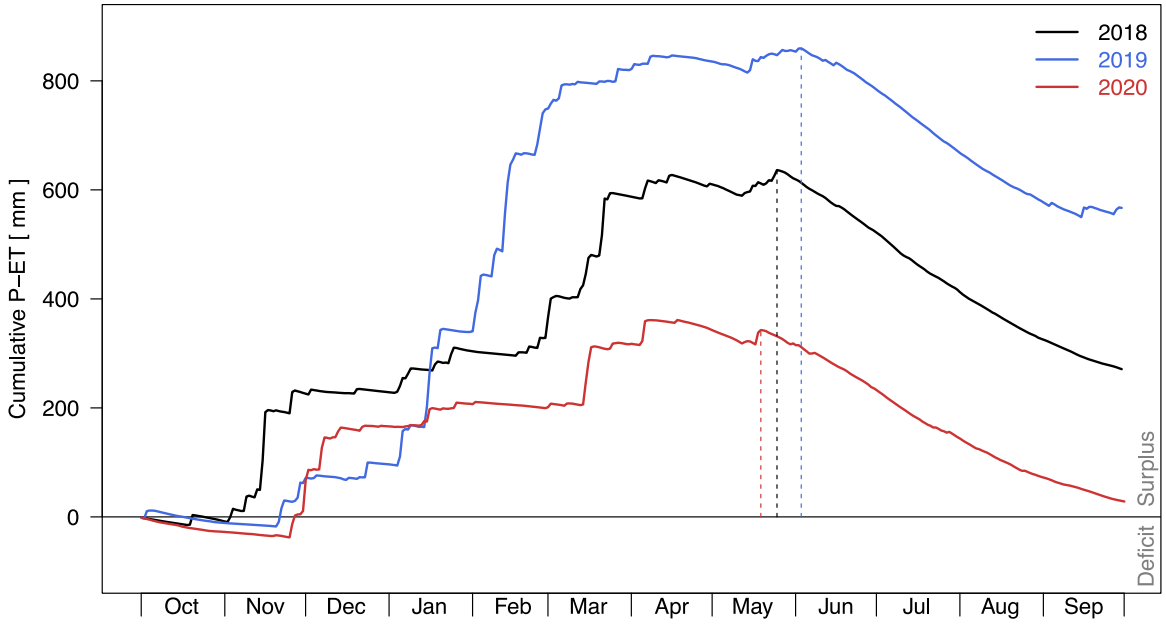

Fig. 9. Cumulative daily precipitation (P) minus evapotranspiration (ET) across water years (Oct–Sep) for above-canopy measured ET at Sagehen. Vertical lines denote the onset of persistent dry season decline.

4. Discussion

4.1. ET comparison across the Sierra Nevada

While Sagehen is, to our knowledge, the only EC site on the east side of the Sierra Nevada, the measured annual ET rates can be compared to other sites located on the west side or in the foothills of the Sierra Nevada (Table 2). However, this requires a consideration of differences in climate (*i.e.* temperature and precipitation) that are largely related to elevation across the Sierra Nevada. Across seven Sierra Nevada sites (Table 2), precipitation ranges from 500 to 600 mm yr^{-1} in the foothills (elevation of 129–405 m a.s.l.) to almost 1400 mm yr^{-1} at elevations of 1300–2000 m a.s.l. on the western slope of the Sierra Nevada, whereas Sagehen on the east side receives only 800–900 mm yr^{-1} of precipitation at a similar elevation of ~1900 m a.s.l. (Table 2). Sagehen is also by far the coldest of these sites (annual average ~5° C), while those on the west side are much warmer at similar elevations (8.6° C) and particularly in the foothills (16–18° C). In other words, Sagehen on the east side is an outlier compared to the strong climate-elevation relationships on the west side of the Sierra Nevada, where annual precipitation increases by about 100 mm yr^{-1} with every degree decrease in mean annual temperature (R^2=0.93, linear regression analysis), or increases by ~50 mm yr^{-1} with every 100 m of elevation gain (R^2=0.87).

Across sites in the Sierra Nevada, annual totals of ET range from about 300 to 900 mm yr^{-1} (Table 2) and more than two-thirds of the variability (R^2=0.78, linear regression analysis) is explained by precipitation and one-third by a relationship with temperature (see also Goulden and Bales, 2014), which are both related to elevation and site location on the east or west side of the Sierra. At Sagehen, we found ET values similar to those reported from a mixed forest at Soaproot Saddle (658 mm yr^{-1}) and an evergreen needleleaf forest at Providence (644 mm yr^{-1}) on the western slope (Rungee et al., 2019). In comparison, much lower rates of annual ET measured by EC (324–419 mm yr^{-1}) were reported for woodlands and grasslands in the western foothills of the Sierra Nevada. Among these sites is the most comprehensive record (18 years) of ET observations in California, including concurrent below-canopy measurements in the oak woodland at Tonzi Ranch (Ma et al., 2020b). Below-canopy contributions from grasses at Tonzi were about 40% (or 167 ± 36 mm yr^{-1}) of above-canopy ET_{Above} measured during 2002–2019, and oak T_{Tree} was reported as 281 ± 48 mm yr^{-1} (Ma et al., 2020b). Although Tonzi is located at much lower elevation (169 m a.s.l.) with warmer temperatures and lower precipitation on the west side of the Sierra (see Table 2), we observed similar understory contributions of about 46% and annual T of 331 ± 33 mm yr^{-1} for Lodgepole pine at Sagehen during 2018–2020 (see Table 1 and *Section 3.6*). This resemblance in T_{Tree} seems linked to groundwater access by deep roots of the oak trees at Tonzi (Ma et al., 2016), similar to the access to near-surface groundwater that trees enjoy at our Sagehen site. Due to its location near the creek in the lower catchment, our Sagehen site is less water-limited than Tonzi (based on the Dryness Index); although both sites have similar potential evapotranspiration (PET) of 1250–1300 mm yr^{-1}, Sagehen's ratio of actual to potential ET (47%) is higher than Tonzi's (34%; see Table 2). The closest site to Sagehen with EC-measured annual ET is Blodgett Forest (~70 km), a Ponderosa pine plantation with Whiteleaf manzanita in the understory and a reported mean ET_{Above} of 892 mm yr^{-1} for the period 1998–2007 (Rungee et al., 2019). However, Blodgett is located on the western side of the Sierra Nevada at a substantially lower elevation (1315 m a.s.l.), with warmer temperatures (11.4° C) and higher amounts of P (1341 mm yr^{-1}). A mixed conifer forest at Providence, with a similar elevation (2015 m a.s.l.) yet warmer temperatures further South on the western side of the Sierra Nevada, required about 50% more annual P to sustain an annual ET similar to Sagehen's (see Table 2). At Sagehen, it has been shown that groundwater hydraulic gradients point towards the creek, indicating a groundwater subsidy to the creek and near-creek environment, driven by seepage from the surrounding uplands (Kirchner et al., 2020). Accordingly, the creek and nearby areas have no water limitations for ET during summer (see Figs. 3 & 7) and it seems reasonable to assume that the measured ET of ~600 mm yr^{-1} at Sagehen is among the highest possible rates for forest ET at about 2000 m elevation on the east side of the Sierra Nevada. The same seems to apply for the measured ET_{Below} of 275 mm yr^{-1} (or 46% of total ET_{Above}) at Sagehen for the understory of montane forest in the Mediterranean climate of California because (i) there is constantly available water near the creek throughout the dry season, (ii) the density of the forest canopy is relatively low (LAI of 1.6) and thus the available energy in the understory is relatively high, and (iii) the understory vegetation is dense (total forest LAI of 3.6 including grasses, see Section 2.7).

In addition to measurements for specific sites, several studies quantified ET for the Sierra Nevada combining models, remote sensing and EC measurements, reporting overall lower annual ET compared to our Sagehen site. Annual ET across the Sierra Nevada mountains was reported as 396 ± 24 mm yr^{-1} for the period 2001–2017 based on a biophysical model informed by remote sensing observations (Baldocchi et al., 2019). For the upper King River Basin (western slope of the Southern Sierra Nevada), EC measurements extrapolated with remote sensing yielded ET estimates of 429 mm yr^{-1} for the period 2003–2011 (Goulden et al., 2012). While P in the King River Basin (P of 984 mm yr^{-1}) was about 20% higher than at Sagehen (1981–2010, see Table 1), the ~40% higher ET measured at our Sagehen site seems related to the lack of water limitations in summer due to its location by the creek in the lower catchment. Similar to measurements in the King River Basin (Goulden et al., 2012), interannual variability of ET was relatively small (*i.e.* 606 ± 50 mm yr^{-1}) at Sagehen during 2018–2020. For the larger region, a synthesis across seven flux tower sites with evergreen needleleaf forests in the semiarid western US reported an average ET of 660 ± 230 mm yr^{-1} (Rungee et al., 2019), which is similar to the ET measured at Sagehen. While no reductions in ET related to drought from precipitation deficits were reported from these evergreen needleleaf forests (Rungee et al., 2019) and only minor reductions were observed at Sagehen during the dry year 2020 (see Fig. 5 and *Section 3.1*), disturbance-related ET reductions have been reported from reduced

Table 2
Comparison of average air Temperature (Tair), precipitation (P), evapotranspiration (ET), potential evapotranspiration (PET), dryness index (DI = PET/P, DI>1 = water limited, DI<1 = energy limited) and evaporative index (EI = ET/P) for eddy covariance flux tower sites in the Sierra Nevada mountains of California. Apart from Sagehen, data were compiled from Rungee et al., 2019, Rungee et al. 2020, and Ma et al. 2020b. Please note that all sites are located on the western slope of the Sierra Nevada Mountains, except Sagehen on the East side. See *Section 2.1* for details concerning the two IGBP classes WSA/ENF at Sagehen.

Site Name	Site ID	Lat. [°]	Long. [°]	Elevation [m]	IGBP	Water Years	Tair [° C]	P [mm]	ET [mm]	PET [mm]	P-ET [mm]	DI	EI
Sagehen	US-SHC	39.43	–120.24	1934	WSA/ENF	2018–2020	5.2	895	606	1299	289	1.45	0.68
Blodgett	US-Blo	38.90	–120.63	1315	ENF	1998–2007	11.4	1341	892	1282	449	0.96	0.67
Tonzi Ranch	US-Ton	38.43	–121.00	169	WSA	2002–2019	16.3	563	419	1246	144	2.21	0.74
Vaira Ranch	US-Var	38.41	–120.95	129	GRA	2001–2018	15.8	592	324	903	268	1.53	0.55
San Joaquin	US-CZ1	37.11	–119.73	405	WSA	2011–2015	17.7	502	378	1402	124	2.79	0.75
Soaproot Saddle	US-CZ2	37.03	–119.26	1160	MF	2011–2015	13.5	934	658	1525	276	1.63	0.70
Providence	US-CZ3	37.07	–119.20	2015	ENF	2009–2015	8.6	1379	644	1098	735	0.80	0.47

vegetation water use due to tree mortality from bark beetle infestation (Goulden and Bales, 2019) and due to wildfires (Ma et al., 2020a) across the Sierra Nevada.

4.2. P-ET water balance

The concurrent EC measurements at our Sagehen site covered a large range in precipitation (*i.e.* 579–1186 mm yr^{-1}) and thus a large range in water supply from the atmosphere across the water years 2018–2020. However, the measured annual rates of ET varied by only about ± 8% (606 ± 50 mm yr^{-1}) and ± 6% (275 ± 17 mm yr^{-1}) above and below the canopy, respectively, and partitioned T_{Tree} varied by only ± 10% (331 ± 33 mm yr^{-1}). In other words, total ET at Sagehen was largely decoupled from annual P, because at this location near the stream, soil water supply is maintained by groundwater seepage toward the valley axis (Kirchner et al., 2020).

We found a consistent pattern of dry-season decline in P–ET that indicates similar vegetation water use across years. Shifts in the onset of this decline were related to the snowpack's melt-out date (in late April or early May) and the associated peak of vegetation activity, which resulted in increasing ET during late spring. The drier the year was (*i.e.* the lower the winter P), the earlier the dry-season decline began (see Fig. 9). During the exceptionally dry year of 2020, the measured P–ET water balance at Sagehen became relatively close to zero. As the tower site is a relatively wet location in the lower catchment and precipitation water supply was reduced everywhere in the region, there were likely substantial water deficits across the basin during that year.

The P–ET water balance at Sagehen is typically positive in the order of ~270 mm yr^{-1} during average years, reflecting the wet location in the lower catchment. While Sagehen is the only site with measured P–ET on the east side of the Sierra, some climate-related patterns are evident from sites on the western slope (see Table 2). Regressing the annual P–ET water balance with mean annual temperature showed a consistent linear relationship across sites on the western slope of the Sierra Nevada (R^2=0.93), while Sagehen appeared as an outlier (R^2=0.37 including Sagehen, see Table 2 for data). This is likely related to two factors: (i) Sagehen is located on the east side with overall lower precipitation compared to the west side (leeward shadow effect), and (ii) measured ET at our Sagehen site is most likely higher than elsewhere with similar elevation and climate conditions due to the wet location near the creek in the lower catchment. A similar consistent P–ET relationship with temperature was reported for basin-wide watershed ET (derived as P–Q, with Q = net subsurface and overland flow) across the western slope of the Sierra Nevada, which has been interpreted as implying increasing montane ET with climate warming (Goulden and Bales, 2014). No such analysis has been reported for the eastern slope of the Sierra Nevada so far, but it can be assumed that a similar pattern might apply.

4.3. Environmental controls on ET

For the environmental controls of ET rates at Sagehen, we found a much stronger relationship with *AE* from radiative measurements (*i.e.* R_N-G) for the below-canopy measurements (75%) than for the above-canopy measurements (52%, see *Section 3.4*). The weaker relationship of *AE* with ET_{Above} seems linked to the heterogeneity of the vegetation within the footprint of the measured fluxes. More specifically, the above-canopy tower (AC) is surrounded by an open meadow that is largely seen by the radiative measurements (*i.e.* R_N and G), while the turbulent measurements are dominated by the forest (see Fig. 4 and *Section 2.4.3*). In contrast, the source areas of the below-canopy radiative and turbulent measurements are more similar to one another. Our results suggest that averaged AE (*i.e.* R_N and G) from concurrent measurements above and below the canopy are more representative than just above-canopy measurements for explaining the variability in total ecosystem ET at Sagehen, and likely in other forest ecosystems as well. This indicates the importance of sufficiently sampling the heterogeneity in forest ecosystems and the benefit of additional below-canopy measurements to investigate the strength of environmental controls for forest ET

4.4. Understory ET contributions

Using a paired setup of two below-canopy towers for turbulent measurements, we found that the spatial variability of daily ET_{Below} at Sagehen was relatively small (about 11%, see Fig. 6) and thus the annual totals at both locations were similar (see *Section 3.5*), despite the heterogeneity in tree density. Previous research indicated that uncertainties in spatial variability were roughly 5–10% for a horizontal separation of 30–50 m in the understories of a closed deciduous forest (Wilson and Meyers, 2001) and a boreal aspen forest (Yang et al., 1999), with both studies suggesting decreasing differences between locations with longer measurement periods. These findings combined with our results from Sagehen suggest overall small spatial variability in below-canopy forest ET, at least at the scale of below-canopy tower footprints and as long as the understory vegetation and environmental conditions are similar.

Despite the rigorous data screening procedures and the regular cleaning of instrumentation at Sagehen (see *Sections 2.2 & 2.3*), we consider the EC measurements at the below-canopy towers to have a relatively high uncertainty during winter. This is due to (i) snow coverage reducing the ground-to-sensor distance and thus damping the turbulent exchange, (ii) a larger number of data gaps during winter related to sensor obstruction (both optical and physical), reduced turbulent exchange and more stable atmospheric stratification, and (iv) the generally low measured fluxes that are near the detection limit during the winter season.

4.5. Tree T and T/ET ratio

The tree T/ET ratio observed at Sagehen (47%) was lower than the 67–95% reported from other forests based on concurrent above- and below-canopy EC measurements to estimate T (Black et al., 1996; Ma et al., 2020b; Paul-Limoges et al., 2020; Roupsard et al., 2006; Sulman et al., 2016; Wilson et al., 2001). Including understory vegetation in the T/ET ratio at our Sagehen site (67–74%) resulted in similar values to the 67 ± 8% reported over 18 years in a Californian oak-grass savanna in the foothills on the western slope of the Sierra Nevada at Tonzi Ranch (Ma et al., 2020b). Although Sagehen is a coniferous forest, the vegetation rather resembles a woody savanna (see *Section 2.1*) and thus has some similarity to the Tonzi site. The main reason for the lower T/ET ratio just based on trees at Sagehen seems linked to the constant water availability near the creek and thus to higher understory contributions, particularly from the persistently green grasses during the summer growing season (see Fig. 8). This becomes evident when comparing the dry season tree T/ET of 44% for Sagehen with >90% for Tonzi, where grasses become fully senescent due to water limitations and thus ET_{Above} is largely dominated by T_{Tree} during summer. The total T/ET ratio of 67–74% (including trees and understory vegetation) at our Sagehen site was also close to 74% reported for a temperate mixed forest in Switzerland with senescent understory vegetation during summer (Paul-Limoges et al., 2020), 85% for an uneven-aged mixed deciduous forest in the Southeastern US (Wilson et al., 2001), and 71% for a boreal aspen forest, rising to 95% when $T_{Understory}$ from the hazelnut understory is included (Black et al., 1996).

Another, but probably smaller, factor influencing the reported T/ET ratios is the potential bias from canopy interception, which is not considered by most studies. Our estimate of total tree canopy interception at Sagehen was about 7% of ET and 5% of P (see Table S2), which are higher than the reported 2–4% for oak-grass savanna at Tonzi Ranch (Ma et al., 2020b). We are nonetheless confident in our interception estimates at Sagehen, because most of the P (causing interception) occurs during the wet winter season (89 ± 3%) as snow, thus having higher interception losses compared to rain, and additionally because most ET occurs during the dry summer season (80% and 82% for below

and above canopy, respectively).

5. Conclusions

Using concurrent above- and below-canopy EC measurements of ET at Sagehen, we show the potential of this approach for quantifying sources of biosphere-atmosphere water exchange within forests, and for partitioning the component fluxes of E and T. The concurrent measurement setup enabled us to detect decoupling of above- and below-canopy turbulent exchange. Our measurements at two similar understory locations suggest that the spatial variability of below-canopy ET is relatively small near the creek at our Sagehen site. These results suggest that below-canopy measurements will primarily depend on environmental conditions (mainly water availability and radiation) and forest structure (*i.e.* tree density and vegetation composition), rather than the exact locations where those measurements are made. Despite large variability in precipitation totals during 2018–2020, the interannual variability in ET and T at Sagehen was small, reflecting persistent water availability and stable vegetation water use in the riparian zone of the lower catchment at Sagehen. Most of the total annual ET at Sagehen occurred during the summer dry season, with understory contributions dominating during the months of June to August and forest canopy (tree) contributions dominating during the remainder of the year, in particular during the snow-covered period. Transpiration from trees accounted for just 47% of total forest ET at Sagehen, whereas transpiration from the canopy and understory vegetation combined was 67–74% of total forest ET. The ET rates measured at our Sagehen site are most likely near the upper limit for coniferous montane forests in the eastern Sierra Nevada, due to the wet location near the creek in the lower catchment.

CRediT authorship contribution statement

Sebastian Wolf: Conceptualization, Data curation, Formal analysis, Investigation, Methodology, Project administration, Validation, Visualization, Writing – original draft, Writing – review & editing. **Eugénie Paul-Limoges:** Conceptualization, Investigation, Methodology, Writing – original draft, Writing – review & editing. **Dan Sayler:** Data curation, Investigation, Project administration, Resources, Writing – review & editing. **James W. Kirchner:** Conceptualization, Funding acquisition, Investigation, Methodology, Project administration, Resources, Supervision, Writing – original draft, Writing – review & editing.

Declaration of Competing Interest

The authors declare that they have no known competing financial interests or personal relationships that could have appeared to influence the work reported in this paper.

Data availability

Data used in this paper are available in the data repositories of AmeriFlux (http://ameriflux.lbl.gov) and the PhenoCam network (https://phenocam.nau.edu), or upon request to the corresponding author.

Acknowledgements

This research was funded by ETH Zurich. E.P-L. acknowledges support by the MainWood project (ETH Domain Joint Initiatives 2023–2026). We acknowledge support for the implementation of our measurements by the former Sagehen station managers Jeff Brown, Faerthern Felix and Ash Zemenick. We further appreciate the help by numerous graduate students, researchers and technical staff from the University of Nevada, Reno during the installation and maintenance of instrumentation at Sagehen, including essential network support by David Slater. The EC measurements at Sagehen were supported by AmeriFlux through the provision of calibration gases. Data used in this paper are available in the data repositories of AmeriFlux (http://ameriflux.lbl.gov) and the PhenoCam network (https://phenocam.nau.edu), or upon request to the corresponding author. We thank the editors and anonymous reviewers for their suggestions to improve the manuscript.

Supplementary materials

Supplementary material associated with this article can be found, in the online version, at doi:10.1016/j.agrformet.2023.109864.

References

Abbott, B.W., et al., 2019. Human domination of the global water cycle absent from depictions and perceptions. Nat. Geosci. 12 (7), 533–540.
Anderegg, W.R.L., et al., 2016. Meta-analysis reveals that hydraulic traits explain cross-species patterns of drought-induced tree mortality across the globe. Proc. Natl. Acad. Sci. 113 (18), 5024–5029.
Baldocchi, D., 1997. Flux footprints within and over forest canopies. Boundary Layer Meteorol. 85 (2), 273–292.
Baldocchi, D., Dralle, D., Jiang, C., Ryu, Y., 2019. How much water is evaporated across California? A multiyear assessment using a biophysical model forced with satellite remote sensing data. Water Resour. Res. 55 (4), 2722–2741.
Baldocchi, D.D., Hincks, B.B., Meyers, T.P., 1988. Measuring biosphere-atmosphere exchanges of biologically related gases with micrometeorological methods. Ecology 69 (5), 1331–1340.
Baldocchi, D.D., Law, B.E., Anthoni, P.M., 2000. On measuring and modeling energy fluxes above the floor of a homogeneous and heterogeneous conifer forest. Agric. For. Meteorol. 102 (2–3), 187–206.
Baldocchi, D.D., Ryu, Y., 2011. A synthesis of forest evaporation fluxes – from days to years – as measured with eddy covariance (Editors). In: Levia, D.F.F., Carlyle-Moses, D., Tanaka, T. (Eds.), Forest Hydrology and Biogeochemistry. Ecological Studies. Springer, Netherlands, pp. 101–116.
Baldocchi, D.D., Vogel, C.A., Hall, B., 1997. Seasonal variation of energy and water vapor exchange rates above and below a boreal jack pine forest canopy. J. Geophys. Res. Atmos. 102 (D24), 28939–28951.
Baldocchi, D.D., Xu, L., Kiang, N., 2004. How plant functional-type, weather, seasonal drought, and soil physical properties alter water and energy fluxes of an oak–grass savanna and an annual grassland. Agric. For. Meteorol. 123 (1–2), 13–39.
Berkelhammer, M., et al., 2016. Convergent approaches to determine an ecosystem's transpiration fraction. Glob. Biogeochem. Cycles 30 (6), 933–951.
Betts, R.A., et al., 2007. Projected increase in continental runoff due to plant responses to increasing carbon dioxide. Nature 448 (7157), 1037–1041.
Black, T.A., et al., 1996. Annual cycles of water vapour and carbon dioxide fluxes in and above a boreal aspen forest. Glob. Chang. Biol. 2 (3), 219–229.
Black, T.A., Kelliher, F.M., 1989. Processes controlling understorey evapotranspiration. Philosophical transactions of the royal society of London. Series B, Biol. Sci. 324 (1223), 207–231.
Blanken, P.D., et al., 2001. The seasonal water and energy exchange above and within a boreal aspen forest. J. Hydrol. (Amst) 245 (1), 118–136.
Brunet, Y., 2020. Turbulent flow in plant canopies: historical perspective and overview. Boundary Layer Meteorol. 177 (2), 315–364.
Burns, S.P., et al., 2014. Snow temperature changes within a seasonal snowpack and their relationship to turbulent fluxes of sensible and latent heat. J. Hydrometeorol. 15 (1), 117–142.
Cao, L., Bala, G., Caldeira, K., Nemani, R., Ban-Weiss, G., 2010. Importance of carbon dioxide physiological forcing to future climate change. Proc. Natl. Acad. Sci. 107 (21), 9513–9518.
Carminati, A., Javaux, M., 2020. Soil rather than xylem vulnerability controls stomatal response to drought. Trends Plant Sci. 25 (9), 868–880.
Čermák, J., Kučera, J., Nadezhdina, N., 2004. Sap flow measurements with some thermodynamic methods, flow integration within trees and scaling up from sample trees to entire forest stands. Trees 18 (5), 529–546.
Chi, J., et al., 2021. Forest floor fluxes drive differences in the carbon balance of contrasting boreal forest stands. Agric. For. Meteorol. 306, 108454.
Choat, B., et al., 2012. Global convergence in the vulnerability of forests to drought. Nature 491 (7426), 752–755.
Constantin, J., Grelle, A., Ibrom, A., Morgenstern, K., 1999. Flux partitioning between understorey and overstorey in a boreal spruce/pine forest determined by the eddy covariance method. Agric. For. Meteorol. 98-99, 629–643.
Cooper, A.E., et al., 2020. Snowmelt causes different limitations on transpiration in a Sierra Nevada conifer forest. Agricul. Forest Meteorol. 291, 108089.
Denmead, O.T., Bradley, E.F., 1985. Flux-Gradient Relationships in a Forest Canopy (Editors). In: Hutchison, B.A., Hicks, B.B. (Eds.), The Forest-Atmosphere Interaction: Proceedings of the Forest Environmental Measurements Conference Held At Oak Ridge, Tennessee, October 23–28, 1983. Springer, Netherlands, Dordrecht, pp. 421–442.

D'Orangeville, L., et al., 2016. Northeastern North America as a potential refugium for boreal forests in a warming climate. Science 352 (6292), 1452–1455.
Feigenwinter, C., et al., 2008. Comparison of horizontal and vertical advective CO2 fluxes at three forest sites. Agric. For. Meteorol. 148 (1), 12–24.
Finnigan, J., 2000. Turbulence in plant canopies. Annu. Rev. Fluid Mech. 32, 519–571.
Fisher, J.B., et al., 2017. The future of evapotranspiration: global requirements for ecosystem functioning, carbon and climate feedbacks, agricultural management, and water resources. Water Resour. Res. 53 (4), 2618–2626.
Fisher, J.B., Whittaker, R.J., Malhi, Y., 2011. ET come home: potential evapotranspiration in geographical ecology. Global Ecol. Biogeogr. 20 (1), 1–18.
Foken, T., 2008. The energy balance closure problem: an overview. Ecol. Appl. 18 (6), 1351–1367.
Foken, T., Leuning, R., Oncley, S.R., Mauder, M., Aubinet, M., 2012. Corrections and data quality control (Editors). In: Aubinet, M., Vesala, T., Papale, D. (Eds.), Eddy Covariance: A Practical Guide to Measurement and Data Analysis. Springer, Netherlands, Dordrecht, pp. 85–131.
Foken, T., Wichura, B., 1996. Tools for quality assessment of surface-based flux measurements. Agric. For. Meteorol. 78 (1–2), 83–105.
Gobin, R., Korboulewsky, N., Dumas, Y., Balandier, P., 2015. Transpiration of four common understorey plant species according to drought intensity in temperate forests. Ann. For. Sci. 72 (8), 1053–1064.
Goulden, M.L., et al., 2012. Evapotranspiration along an elevation gradient in California's Sierra Nevada. J. Geophys. Res. 117 (G3), G03028.
Goulden, M.L., Bales, R.C., 2014. Mountain runoff vulnerability to increased evapotranspiration with vegetation expansion. Proc. Natl. Acad. Sci. 111 (39), 14071–14075.
Goulden, M.L., Bales, R.C., 2019. California forest die-off linked to multi-year deep soil drying in 2012–2015 drought. Nat. Geosci. 12 (8), 632–637.
Hirschi, M., Michel, D., Lehner, I., Seneviratne, S.I., 2017. A site-level comparison of lysimeter and eddy covariance flux measurements of evapotranspiration. Hydrol. Earth Syst. Sci. 21 (3), 1809–1825.
Huntington, T.G., 2006. Evidence for intensification of the global water cycle: review and synthesis. J. Hydrol. (Amst) 319 (1–4), 83–95.
Iida, S.i., et al., 2009. Evapotranspiration from understory vegetation in an eastern Siberian boreal larch forest. Agric. For. Meteorol. 149 (6), 1129–1139.
Iida, S.i., et al., 2020. Evapotranspiration from the understory of a tropical dry deciduous forest in Cambodia. Agric. For. Meteorol. 295, 108170.
Jarosz, N., et al., 2008. Carbon dioxide and energy flux partitioning between the understorey and the overstorey of a maritime pine forest during a year with reduced soil water availability. Agric. For. Meteorol. 148 (10), 1508–1523.
Jocher, G., et al., 2017. Apparent winter CO2 uptake by a boreal forest due to decoupling. Agric. For. Meteorol. 232, 23–34.
Jocher, G., et al., 2018. Impact of canopy decoupling and subcanopy advection on the annual carbon balance of a boreal scots pine forest as derived from eddy covariance. J. Geophys. Res. 123 (2), 303–325.
Johnson, C.M., Needham, P.R., 1966. Ionic composition of Sagehen Creek, California, following an adjacent fire. Ecology 47 (4), 636–639.
Kaimal, J.C., Finnigan, J.J., 1994. Atmospheric Boundary Layer flows: Their Structure and Measurement. Oxford University Press, New York, p. 289.
Kaimal, J.C., Wyngaard, J.C., Izumi, Y., Coté, O.R., 1972. Spectral characteristics of surface-layer turbulence. Q. J. R. Meteorolog. Soc. 98 (417), 563–589.
Kannenberg, S.A., et al., 2022. Opportunities, challenges and pitfalls in characterizing plant water-use strategies. Funct. Ecol. 36 (1), 24–37.
Kassuelke, S.R., Dymond, S.F., Feng, X., Savage, J.A., Wagenbrenner, J.W., 2022. Understory evapotranspiration rates in a coast redwood forest. Ecohydrology 15 (3), e2404.
Kauffman, E., 2003. Climate and Topography, Atlas of the Biodiversity of California California Department of Fish and Game. Sacramento, California, pp. 12–15.
Keenan, T.F., et al., 2013. Increase in forest water-use efficiency as atmospheric carbon dioxide concentrations rise. Nature 499 (7458), 324–328.
Kelliher, F.M., et al., 1997. Evaporation from an eastern Siberian larch forest. Agric. For. Meteorol. 85 (3), 135–147.
Kelliher, F.M., et al., 1998. Evaporation from a central Siberian pine forest. J. Hydrol. (Amst) 205 (3), 279–296.
Kilinc, M., Beringer, J., Hutley, L.B., Tapper, N.J., McGuire, D.A., 2013. Carbon and water exchange of the world's tallest angiosperm forest. Agric. For. Meteorol. 182-183, 215–224.
Kirchner, J.W., et al., 2020. The pulse of a montane ecosystem: coupling between daily cycles in solar flux, snowmelt, transpiration, groundwater, and streamflow at Sagehen Creek and Independence Creek. Sierra Nevada, USA. Hydrol. Earth Syst. Sci. 24 (11), 5095–5123.
Kljun, N., Calanca, P., Rotach, M.W., Schmid, H.P., 2015. A simple two-dimensional parameterisation for Flux Footprint Prediction (FFP). Geosci. Model. Dev. 8 (11), 3695–3713.
Knauer, J., et al., 2018. Towards physiologically meaningful water-use efficiency estimates from eddy covariance data. Glob. Chang. Biol. 24 (2), 694–710.
Launiainen, S., et al., 2005. Eddy covariance measurements of CO2 and sensible and latent heat fluxes during a full year in a boreal pine forest trunk-space. Environ Res 10 (6), 569–588.
Launiainen, S., 2010. Seasonal and inter-annual variability of energy exchange above a boreal Scots pine forest. Biogeosciences 7 (12), 3921–3940.
Leuning, R., van Gorsel, E., Massman, W.J., Isaac, P.R., 2012. Reflections on the surface energy imbalance problem. Agric. For. Meteorol. 156 (0), 65–74.
Lian, X., Zhao, W., Gentine, P., 2022. Recent global decline in rainfall interception loss due to altered rainfall regimes. Nat. Commun. 13 (1), 7642.
Liu, Z., Wang, Y., Yu, P., Xu, L., Yu, S., 2022. Environmental and canopy conditions regulate the forest floor evapotranspiration of larch plantations. Forest Ecosyst. 9, 100058.
Ma, Q., et al., 2020a. Wildfire controls on evapotranspiration in California's Sierra Nevada. J. Hydrol. (Amst) 590, 125364.
Ma, S., Baldocchi, D., Wolf, S., Verfaillie, J., 2016. Slow ecosystem responses conditionally regulate annual carbon balance over 15 years in Californian oak-grass savanna. Agric. For. Meteorol. 228–229, 252–264.
Ma, S., Eichelmann, E., Wolf, S., Rey-Sanchez, C., Baldocchi, D.D., 2020b. Transpiration and evaporation in a Californian oak-grass savanna: field measurements and partitioning model results. Agric. For. Meteorol. 295, 108204.
Manning, A.H., et al., 2012. Evolution of groundwater age in a mountain watershed over a period of thirteen years. J. Hydrol. (Amst) 460-461, 13–28.
Massman, W.J., 2000. A simple method for estimating frequency response corrections for eddy covariance systems. Agric. For. Meteorol. 104 (3), 185–198.
Massman, W.J., 2001. Reply to comment by Rannik on "A simple method for estimating frequency response corrections for eddy covariance systems. Agric. For. Meteorol. 107 (3), 247–251.
Mast, A., Clow, D.W., 2000. Environmental characteristics and water quality of hydrologic benchmark network stations in the western United States 1963-95, 1173D.
Mauder, M., et al., 2008. Quality control of CarboEurope flux data - Part 2: inter-comparison of eddy-covariance software. Biogeosciences 5 (2), 451–462.
Miralles, D.G., Gash, J.H., Holmes, T.R.H., de Jeu, R.A.M., Dolman, A.J., 2010. Global canopy interception from satellite observations. J. Geophys. Res. 115 (D16), D16122.
Misson, L., et al., 2007. Partitioning forest carbon fluxes with overstory and understory eddy-covariance measurements: a synthesis based on FLUXNET data. Agric. For. Meteorol. 144 (1–2), 14–31.
Moncrieff, J., Clement, R., Finnigan, J., Meyers, T., 2004. Averaging, detrending, and filtering of eddy covariance time series (Editors). In: Lee, X., Massman, W., Law, B. (Eds.), Handbook of Micrometeorology: A Guide For Surface Flux Measurement and Analysis. Springer Netherlands, Dordrecht, pp. 7–31.
Moore, K.E., et al., 1996. Seasonal variation in radiative and turbulent exchange at a deciduous forest in Central Massachusetts. J. Appl. Meteorol. (1988-2005) 35 (1), 122–134.
Nelson, J.A., et al., 2020. Ecosystem transpiration and evaporation: insights from three water flux partitioning methods across FLUXNET sites. Glob. Chang. Biol. 26 (12), 6916–6930.
Nelson, Jacob A., et al., 2018. Coupling water and carbon fluxes to constrain estimates of transpiration: the TEA algorithm. J. Geophys. Res. 123 (12), 3617–3632.
Novick, K., Brantley, S., Miniat, C.F., Walker, J., Vose, J.M., 2014. Inferring the contribution of advection to total ecosystem scalar fluxes over a tall forest in complex terrain. Agric. For. Meteorol. 185, 1–13.
Novick, K.A., Konings, A.G., Gentine, P., 2019. Beyond soil water potential: an expanded view on isohydricity including land–atmosphere interactions and phenology. Plant Cell Environ. 42 (6), 1802–1815.
Ohta, T., et al., 2001. Seasonal variation in the energy and water exchanges above and below a larch forest in eastern Siberia. Hydrol. Process 15 (8), 1459–1476.
Oishi, A.C., Oren, R., Stoy, P.C., 2008. Estimating components of forest evapotranspiration: a footprint approach for scaling sap flux measurements. Agric. For. Meteorol. 148 (11), 1719–1732.
Oki, T., Kanae, S., 2006. Global hydrological cycles and world water resources. Science 313 (5790), 1068–1072.
Or, D., Lehmann, P., Shahraeeni, E., Shokri, N., 2013. Advances in soil evaporation physics—A review. Vadose Zone J. 12 (4), 1–16.
Pan, Y., Birdsey, R.A., Phillips, O.L., Jackson, R.B., 2013. The structure, distribution, and biomass of the world's forests. Annu. Rev. Ecol. Evol. Syst. 44 (1), 593–622.
Paul-Limoges, E., et al., 2020. Partitioning evapotranspiration with concurrent eddy covariance measurements in a mixed forest. Agric. For. Meteorol. 280, 107786.
Paul-Limoges, E., Wolf, S., Eugster, W., Hörtnagl, L., Buchmann, N., 2017. Below-canopy contributions to ecosystem CO2 fluxes in a temperate mixed forest in Switzerland. Agric. For. Meteorol. 247 (Supplement C), 582–596.
Pepin, N., et al., 2015. Elevation-dependent warming in mountain regions of the world. Nat. Clim. Chang. 5 (5), 424–430.
Perez-Priego, O., et al., 2017. Evaluation of eddy covariance latent heat fluxes with independent lysimeter and sapflow estimates in a Mediterranean savannah ecosystem. Agric. For. Meteorol. 236, 87–99.
Perez-Priego, O., et al., 2018. Partitioning eddy covariance water flux components using physiological and micrometeorological approaches. J. Geophys. Res. 123 (10), 3353–3370.
Peters, R.L., et al., 2018. Quantification of uncertainties in conifer sap flow measured with the thermal dissipation method. New Phytol. 219 (4), 1283–1299.
Polonik, P., et al., 2019. Comparison of gas analyzers for eddy covariance: effects of analyzer type and spectral corrections on fluxes. Agric. For. Meteorol. 272-273, 128–142.
Poyatos, R., et al., 2021. Global transpiration data from sap flow measurements: the SAPFLUXNET database. Earth Syst. Sci. Data 13 (6), 2607–2649.
Qubaja, R., et al., 2020. Partitioning evapotranspiration and its long-term evolution in a dry pine forest using measurement-based estimates of soil evaporation. Agric. For. Meteorol. 281, 107831.
Raupach, M.R., Shaw, R.H., 1982. Averaging procedures for flow within vegetation canopies. Boundary Layer Meteorol. 22 (1), 79–90.
Raz-Yaseef, N., Yakir, D., Schiller, G., Cohen, S., 2012. Dynamics of evapotranspiration partitioning in a semi-arid forest as affected by temporal rainfall patterns. Agric. For. Meteorol. 157, 77–85.

Rebmann, C., et al., 2012. Data acquisition and flux calculations (Editors). In: Aubinet, M., Vesala, T., Papale, D. (Eds.), Eddy Covariance: A Practical Guide to Measurement and Data Analysis. Springer Netherlands, Dordrecht, pp. 59–83.
Reichstein, M., et al., 2005. On the separation of net ecosystem exchange into assimilation and ecosystem respiration: review and improved algorithm. Glob. Chang. Biol. 11 (9), 1424–1439.
Richardson, A.D., et al., 2018. Tracking vegetation phenology across diverse North American biomes using PhenoCam imagery. Sci. Data 5, 180028.
Roderick, M.L., Greve, P., Farquhar, G.D., 2015. On the assessment of aridity with changes in atmospheric CO_2. Water Resour. Res. 51 (7), 5450–5463.
Roupsard, O., et al., 2006. Partitioning energy and evapo-transpiration above and below a tropical palm canopy. Agric. For. Meteorol. 139 (3–4), 252–268.
Rungee, J., et al., 2020. Data from: evapotranspiration response to multiyear dry periods in the semiarid western United States. Dryad. https://doi.org/10.6071/M3M660.
Rungee, J., Bales, R., Goulden, M., 2019. Evapotranspiration response to multiyear dry periods in the semiarid western United States. Hydrol. Process 33 (2), 182–194.
Scanlon, T.M., Kustas, W.P., 2012. Partitioning evapotranspiration using an eddy covariance-based technique: improved assessment of soil moisture and land–atmosphere exchange dynamics. Vadose Zone J. 11 (3).
Scanlon, T.M., Sahu, P., 2008. On the correlation structure of water vapor and carbon dioxide in the atmospheric surface layer: a basis for flux partitioning. Water Resour. Res. 44 (10).
Schlesinger, W.H., Jasechko, S., 2014. Transpiration in the global water cycle. Agric. For. Meteorol. 189-190, 115–117.
Scott, R.L., et al., 2003. The understory and overstory partitioning of energy and water fluxes in an open canopy, semiarid woodland. Agric. For. Meteorol. 114 (3–4), 127–139.
Scott, R.L., Biederman, J.A., 2017. Partitioning evapotranspiration using long-term carbon dioxide and water vapor fluxes. Geophys. Res. Lett. 44 (13), 6833–6840.
Seneviratne, I.S., Stöckli, R., et al., 2008. The role of land-atmosphere interactions for climate variability in Europe (Editors). In: Brönnimann, S., et al. (Eds.), Climate Variability and Extremes during the Past 100 Years. Springer Netherlands, Dordrecht, pp. 179–193.
Seyednasrollah, B. et al., 2019. PhenoCam dataset v2.0: vegetation phenology from digital camera imagery, 2000-2018. ORNL Distributed Active Arch. Center.
Skaggs, T.H., Anderson, R.G., Alfieri, J.G., Scanlon, T.M., Kustas, W.P., 2018. Fluxpart: open source software for partitioning carbon dioxide and water vapor fluxes. Agric. For. Meteorol. 253-254, 218–224.
Stoy, P.C., et al., 2013. A data-driven analysis of energy balance closure across FLUXNET research sites: the role of landscape scale heterogeneity. Agric. For. Meteorol. 171–172 (0), 137–152.
Stoy, P.C., et al., 2019. Reviews and syntheses: turning the challenges of partitioning ecosystem evaporation and transpiration into opportunities. Biogeosciences 16 (19), 3747–3775.
Sulman, B.N., Roman, D.T., Scanlon, T.M., Wang, L., Novick, K.A., 2016. Comparing methods for partitioning a decade of carbon dioxide and water vapor fluxes in a temperate forest. Agric. For. Meteorol. 226–227, 229–245.
Sun, X., Onda, Y., Otsuki, K., Kato, H., Gomi, T., 2016. The effect of strip thinning on forest floor evaporation in a Japanese cypress plantation. Agric. For. Meteorol. 216, 48–57.
Suni, T., et al., 2015. The significance of land-atmosphere interactions in the Earth system—ILEAPS achievements and perspectives. Coastal Fluxes Anthropocene 12, 69–84.
Swann, A.L.S., Hoffman, F.M., Koven, C.D., Randerson, J.T., 2016. Plant responses to increasing CO_2 reduce estimates of climate impacts on drought severity. Proc. Natl. Acad. Sci. 113 (36), 10019–10024.
Sylvester, A.G., Raines, G.L., 2017. Geology of the Independence Lake and Hobart Mills 7.5′ quadrangles, Nevada and Sierra counties, California (Editors). In: Gutierrez, C.I., Ferrer, A. (Eds.), California Department of Conservation. Sacramento, CA.
Thomas, C., et al., 2008. Estimating daytime subcanopy respiration from conditional sampling methods applied to mufti-scalar high frequency turbulence time series. Agric. For. Meteorol. 148 (8–9), 1210–1229.
Thomas, C.K., Martin, J.G., Law, B.E., Davis, K., 2013. Toward biologically meaningful net carbon exchange estimates for tall, dense canopies: multi-level eddy covariance observations and canopy coupling regimes in a mature Douglas-fir forest in. Oregon. Agricul. Forest Meteorol. 173, 14–27.
Thrippleton, T., Bugmann, H., Folini, M., Snell, R.S., 2018. Overstorey–understorey interactions intensify after drought-induced forest die-off: long-term effects for forest structure and composition. Ecosystems 21 (4), 723–739.
Vandegehuchte, M.W., Steppe, K., 2013. Sap-flux density measurement methods: working principles and applicability. Funct. Plant Biol. 40 (3), 213–223.
Vickers, D., Mahrt, L., 1997. Quality Control and Flux Sampling Problems for Tower and Aircraft Data. J. Atmos. Oceanic Technol. 14 (3), 512–526.
Walter, H.K., Lieth, H., 1967. Klimadiagramm-Weltatlas. Fischer, Jena.
Way, D.A., Cook, A., Rogers, A., 2021. The effects of rising CO2 concentrations on terrestrial systems: scaling it up. New Phytol. 229 (5), 2383–2385.
Webb, E.K., Pearman, G.I., Leuning, R., 1980. Correction of flux measurements for density effects due to heat and water-vapor transfer. Q. J. R. Meteorolog. Soc. 106 (447), 85–100.
Wilczak, J.M., Oncley, S.P., Stage, S.A., 2001. Sonic anemometer tilt correction algorithms. Boundary Layer Meteorol. 99 (1), 127–150.
Wilson, K.B., Hanson, P.J., Mulholland, P.J., Baldocchi, D.D., Wullschleger, S.D., 2001. A comparison of methods for determining forest evapotranspiration and its components: sap-flow, soil water budget, eddy covariance and catchment water balance. Agric. For. Meteorol. 106 (2), 153–168.
Wilson, K.B., Meyers, T.P., 2001. The spatial variability of energy and carbon dioxide fluxes at the floor of a deciduous forest. Boundary Layer Meteorol. 98 (3), 443–473.
Wolf, S., Eugster, W., Majorek, S., Buchmann, N., 2011. Afforestation of tropical pasture only marginally affects ecosystem-scale evapotranspiration. Ecosystems 14 (8), 1264–1275.
Wolf, S., Paul-Limoges, E., 2023. Drought and heat reduce forest carbon uptake. Nat. Commun. 14 (1), 6217.
Wutzler, T., et al., 2018. Basic and extensible post-processing of eddy covariance flux data with REddyProc. Biogeosci. Discuss. 2018, 1–39.
Yang, P.C., Black, T.A., Neumann, H.H., Novak, M.D., Blanken, P.D., 1999. Spatial and temporal variability of CO2 concentration and flux in a boreal aspen forest. J. Geophys. Res. Atmos. 104 (D22), 27653–27661.
Zhong, F., et al., 2022. Revisiting large-scale interception patterns constrained by a synthesis of global experimental data. Hydrol. Earth Syst. Sci. Discuss. 2022, 1–27.
Zhou, S., Yu, B., Zhang, Y., Huang, Y., Wang, G., 2016. Partitioning evapotranspiration based on the concept of underlying water use efficiency. Water Resour. Res. 52 (2), 1160–1175.